PG
Petroleum Geoscience

Research article

Published online June 18, 2018 https://doi.org/10.1144/petgeo2017-063 | Vol. 25 | 2019 | pp. 131–150

Crustal structure and heat-flow history in the UK Rockall Basin, derived from backstripping and gravity-inversion analysis

Alan M. Roberts[1]*, Andrew D. Alvey[1] & Nick J. Kusznir[1,2]

[1] Badley Geoscience Ltd, North Beck House, North Beck Lane, Spilsby, Lincolnshire PE23 5NB, UK
[2] Department of Earth & Ocean Sciences, University of Liverpool, Liverpool L69 3BX, UK
A.M.R., 0000-0003-4839-0741
* Correspondence: alan@badleys.co.uk

Abstract: Seismic data made available by the UK OGA (Oil & Gas Authority) has been used to constrain a model of crustal structure and heat-flow history for the UK Rockall Basin. Top basement/base sediment has been interpreted around the full extent of the seismic dataset. This has produced a model for the thickness of the sediment fill within the basin which is thicker than previous published estimates.

The new sediment-thickness model has been incorporated into a 3D backstripping study, producing maps of subsidence and thinning factor. Analysis of backstripped subsidence shows the thinning factor reaching peak values of *c.* 0.8–0.85 (β factor >5) in the south-central axial area, reducing in magnitude northwards to *c.* 0.7. The new sediment-thickness model has also been incorporated into a 3D gravity-inversion study, mapping Moho depth, crustal thickness and thinning/stretching factor. The results show crustal-basement thickness reduced to *c.* 6 km, thinning factor *c.* 0.8, in the south-central area, while it spans the range *c.* 6–10 km further north. The results are compatible with previous seismic refraction work in both the UK and Irish sectors of the Rockall Basin. We believe that the extension which created the basin was non-magmatic and that the axial region is underlain by highly-thinned continental crust.

The results from the gravity inversion have been used to make predictions about the top-basement heat-flow history. Heat flow in the basin centre is predicted to have been initially high, reducing with time, associated with cooling of the transient synrift heat-flow anomaly. On the basin flanks heat flow was less variable over time, its magnitude controlled primarily by constant radiogenic heat input from the basement, rather than by the transient geotherm anomaly.

There remain considerable uncertainties associated with our interpretation and analysis. These uncertainties have been addressed with sensitivity analyses.

A regional gravity-inversion model, using the new sediment-thickness data spliced into regional public-domain information, shows that structural and stretching continuity can be mapped at the crustal scale along the full length of the UK/Irish Rockall Basin, contrary to conclusions from some previous studies.

Received 1 June 2017; **revised** 5 February 2018; **accepted** 8 May 2018

The Rockall Basin (also referred to in the literature as the Rockall Trough) is a large, deep-water basin located west of the UK and Ireland. It occupies a significant part of the UK/Ireland Continental Shelf, between the onshore areas to the east and the Atlantic continental margin to the west (Fig. 1). In this paper we will focus on a study and analysis of the northern (UK) Rockall Basin.

As a consequence of geographical remoteness and a relative paucity of good-quality seismic data, the Rockall Basin is probably the least well known and understood of the basins which surround the UK. The UK Oil & Gas Authority (OGA) recently (in 2016) sought to rectify this situation by making a considerable amount of new and legacy seismic data (Fig. 2a) freely available under an Open Government Licence:

- Summary: https://www.ogauthority.co.uk/media/2573/north_rockall_free_subsurface_data.pdf
- Access: https://www.ogauthority.co.uk/data-centre/data-downloads-and-publications/seismic-data/
- Licence: http://www.nationalarchives.gov.uk/doc/open-government-licence/version/3/

We have used an interpretation of the OGA seismic data as input into a 3D quantitative modelling study of the UK Rockall Basin, involving subsidence analysis, gravity inversion and heat-flow prediction. The aim of the study has been to predict crustal-basement structure and stretching/thinning factors from gravity-inversion and subsidence analysis, and then use these results to predict the top-basement heat-flow history within the basin. In this way we aim to further the regional understanding of basin structure and to provide a quantitative framework of benefit to future petroleum-systems analysis in the area.

The Rockall Basin

Age of extension

Although it is geographically located within the UK/Irish Atlantic continental margin (Fig. 1), the Rockall Basin is generally considered to be an older basin than the North Atlantic Ocean to the west, which opened at the end of the Paleocene (*c.* 55 Ma: e.g. White *et al.* 2010). The lack of definitive seismic data and well data has meant that the age of the opening of the Rockall Basin is not yet addressed with certainty or consensus by the existing literature.

The most comprehensive description of the geology of the UK Rockall Basin, together with a review of previous work, is the British Geological Survey Research Report for the area (Hitchen *et al.* 2013). Within this report Ritchie *et al.* (2013, p. 11) stated that:

> Active extension during Late Jurassic to Early Cretaceous times resulted in a fully marine linkage of the Arctic and Atlantic rifts,

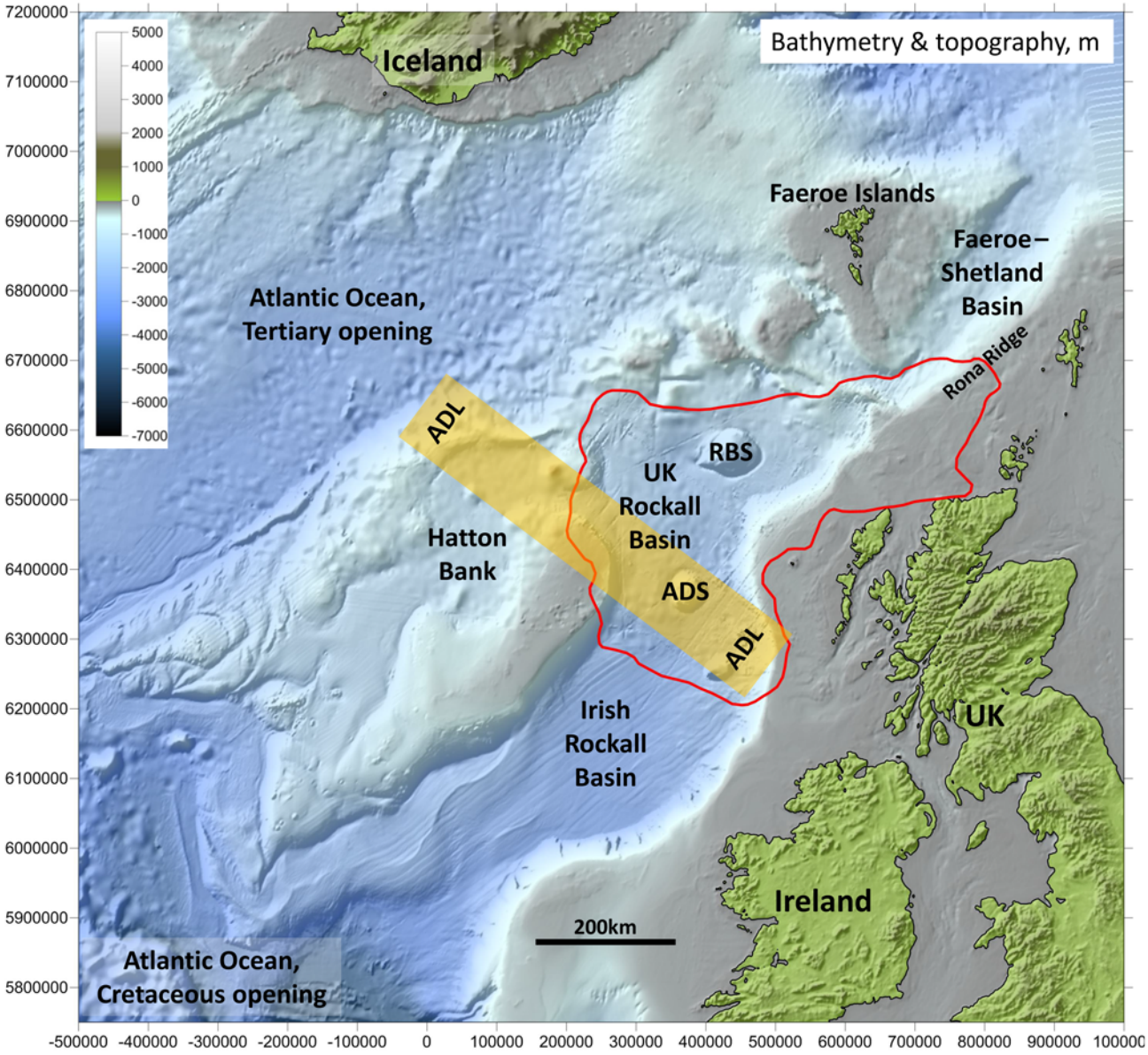

Fig. 1. Shaded-relief bathymetry/topography (Smith & Sandwell 1997; scale in metres) for the UK–Irish Atlantic margin, locating the main geological features referred to in the text. The red polygon encloses the area of the OGA seismic dataset used in the study (Fig. 2). RBS, Rosemary Bank Seamount; ADS, Anton Dohrn Seamount; ADL, Anton Dohrn Lineament; the orange polygon is after Kimbell *et al.* (2005).

creating a continuous rift which is now represented by the Vøring, Møre, Faroe–Shetland and Rockall Basins.

They suggested that Early Cretaceous extension was the 'most major of these' in the Rockall Basin (Ritchie *et al.* 2013, p. 27). Similarly, in a recent summary, Schofield *et al.* (2017, p. 211) stated:

> A Late Jurassic–Early Cretaceous rift phase and Late Cretaceous–Palaeogene post-rift phase appear to characterize much of the stratigraphy of the Rockall Basin (Musgrove & Mitchener 1996; Archer *et al.* 2005).

Following our own interpretation of the OGA seismic data (see below), we base our quantitative modelling of the Rockall Basin on a similar understanding of the likely stretching history.

Others too have reached a similar general conclusion that early-mid Cretaceous extension, preceded by probable Jurassic extension, led to the formation of the Rockall Basin (e.g. England & Hobbs 1997; Cole & Peachey 1999; Nadin *et al.* 1999; Shannon *et al.* 1999). It is worth noting, however, that prior to the emergence of this consensus, Smythe (1989) had argued for a predominantly late Carboniferous–early Permian age for the opening of the basin.

A more recent challenge to the Jurassic-into-Cretaceous extension model has been proposed by Stoker *et al.* (2017). They suggested that the northern (UK) Rockall Basin may be predominantly Late Cretaceous in age, quite probably with no earlier stretching history. It is not our intention here to become involved in the details of the various kinematic models for the opening of the Rockall Basin, but, as we expand upon within this paper, our own interpretation of the OGA seismic data, plus the results of our modelling of crustal structure, lead us to prefer the 'more traditional' Jurassic-into-Cretaceous extension model (e.g. Ritchie *et al.* 2013).

The Rockall Basin is one of a series of contiguous, highly-extended, deep-water basins located along the Irish/UK/Norwegian Atlantic margin (Doré *et al.* 1999; Lundin & Doré 2011, fig. 1), the main extension within which Lundin & Doré (2011) considered to be Early Cretaceous. From south to north, these are the Rockall Basin, the Faeroe–Shetland Basin (Fig. 1), the Møre Basin and the Vøring Basin. We have previously been involved in quantitative

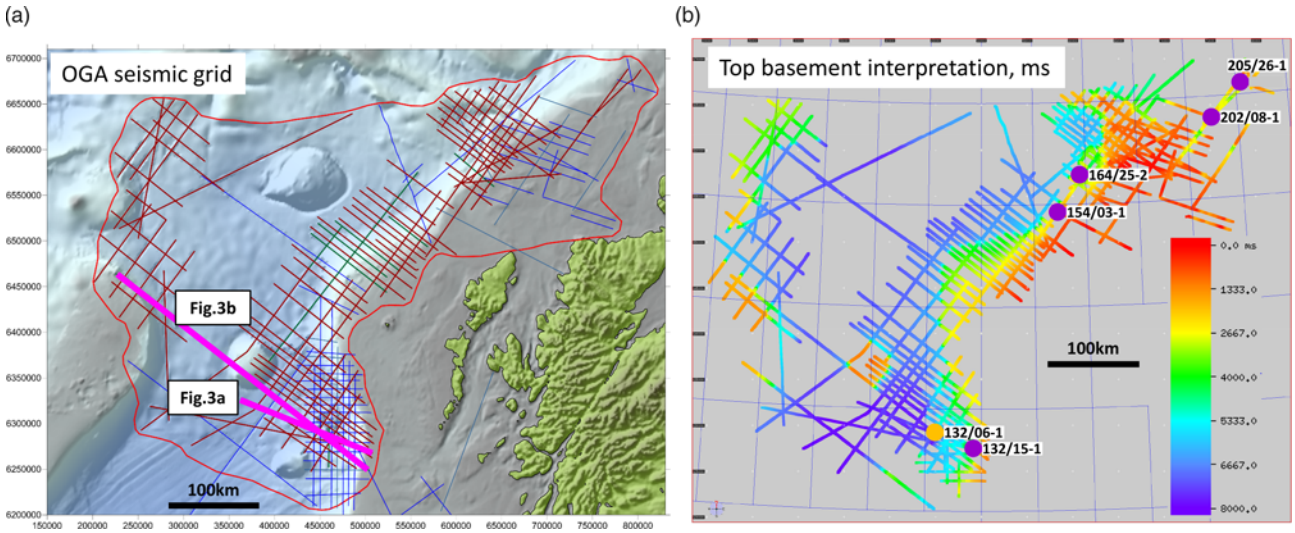

Fig. 2. (**a**) OGA seismic grid used in the study, on shaded-relief bathymetry. Different line colours correspond to different vintage survey elements within the dataset. The two lines illustrated in Figure 3a and b are highlighted. The red polygon is the polygon used in other figures to define the survey area. (**b**) The completed interpretation grid for top basement; the scale in TWT milliseconds (ms). The five wells identified by purple circles are those within the survey area which penetrated top basement and which are tied by the interpretation. 132/15-1 and 132/06-1 (TD Upper Cretaceous) are shown as seismic ties in Figure 3. This seismic grid was interpolated by Kriging and then depth-converted (see the text) to produce the depth map in Figure 4a.

studies of the latter three basins (Roberts *et al.* 1997, 2009; Kusznir *et al.* 2005; Fletcher *et al.* 2013). At its southern (Irish) limit the Rockall Basin is truncated at a high-angle by the younger (here mid-Cretaceous) Atlantic margin (Fig. 1), but was probably originally contiguous across the Atlantic with the West Orphan Basin offshore Newfoundland (e.g. Sibuet *et al.* 2007). North of the Vøring Basin, Lundin & Doré (2011, fig. 1) suggested that this chain of highly-extended basins may continue westwards across the North Atlantic into NE Greenland (Thetis Basin) and then back eastwards across the Atlantic again into the Western Barents Sea of northern Norway (Bjørnoya Basin). Although these deep-water basins sit close to the present-day Atlantic continental margin, they are all older than, and in three places truncated by, the opening of the Atlantic (Lundin & Doré 2011, fig. 1). They record a period of intra-continental rifting and extension which occurred probably *c.* 70–90 myr before the early Tertiary opening of the North Atlantic itself.

Previous crustal-modelling studies

In this paper we investigate the crustal structure of the UK Rockall Basin via seismic interpretation, 3D backstripping and 3D gravity inversion. The most comparable previous study in scope, although covering a much larger area, is that of Kimbell *et al.* (2004), who used gravity modelling supported by backstripping to produce a series of 3D models for the crustal structure of the NE Atlantic margin (offshore Ireland, UK and Norway), within which lies the Rockall Basin. Kimbell *et al.* (2004) presented an extremely thorough analysis, including mapping of crustal thickness and β-stretching factor, which we believe our own more focused study now complements. In discussion of our work below we will highlight similarities to and differences from the work of Kimbell *et al.* The results of the Kimbell *et al.* (2004) study were also used as the basis for further geological discussion of the NE Atlantic margin by Kimbell *et al.* (2005), and are comprehensively summarized and reproduced in Hitchen *et al.* (2013, fig. 16).

Another regional 3D model of crustal structure across the NE Atlantic margin, including the Rockall Basin, was produced by Kelly *et al.* (2007). Their model was constructed from a network of wide-angle seismic-reflection and -refraction profiles (Kelly *et al.* 2007, fig. 1), and populated with information about crustal-velocity structure. Their mapping of depth to Moho was tested and refined against gravity data in addition to seismic constraints. By necessity of the widely-spaced nature of the input seismic lines their crustal model is much coarser (40 × 40 km) than our own subsequent work but is an elegant vehicle for their principal objective of presenting crustal-velocity information in 3D.

In addition to these regional NE Atlantic studies, the crustal structure of the Rockall Basin has been the focus of several wide-angle seismic studies, some of which were incorporated into the input data of Kelly *et al.* (2007). The most comprehensive of these studies is that by Klingelhöfer *et al.* (2005), who investigated two newly-acquired wide-angle seismic lines from the northern UK Rockall Basin (north of Rosemary Bank Seamount: Fig. 1) and integrated this with previously unpublished industry and government seismic data from the same area. They showed that in this northern area crustal basement in the centre of the basin has been thinned to 12–13 km, but on the flanks is substantially thicker at *c.* 25 km. They also showed that their crustal-thickness results were consistent with those obtained previously (further south, between Rosemary Bank and Anton Dohrn seamounts: Fig. 1) by Roberts *et al.* (1988, their profile 2), who acquired the first wide-angle seismic data across the Rockall Basin. Roberts *et al.* (1988) also acquired a second line south of Anton Dohrn Seamount (their profile 5), close to the south of the current study area (Figs 1 and 2). This line resolved crustal basement *c.* 10 km thick in the SE of the basin, but did not resolve a reliable Moho within the basin centre. Also within this southern part of the UK Rockall Basin, Keser Neish (1993) used UK government seismic data to build a composite transect across the Rockall Basin and westwards onto the Atlantic margin. This study showed crustal-basement thickness in the south-centre of the basin to be 6–7 km, rising to *c.* 20 km on either flank.

Further to the south, within the Irish sector of the Rockall Basin, the first published study of deep-crustal structure was that by Joppen & White (1990), who used both seismic reflection and wide-angle refraction data to show that (along their profile SAP-5) crustal-basement thickness in the basin centre is *c.* 6 km, associated with β factors of 6 or more. They suggested that β factors of this magnitude should be associated with 1–3 km of synrift (probably Cretaceous) magmatic addition by decompression melting. Hauser *et al.* (1995) used the early-vintage RAPIDS wide-angle seismic data to demonstrate that, along an axial (NNE–SSW) transect of the Irish

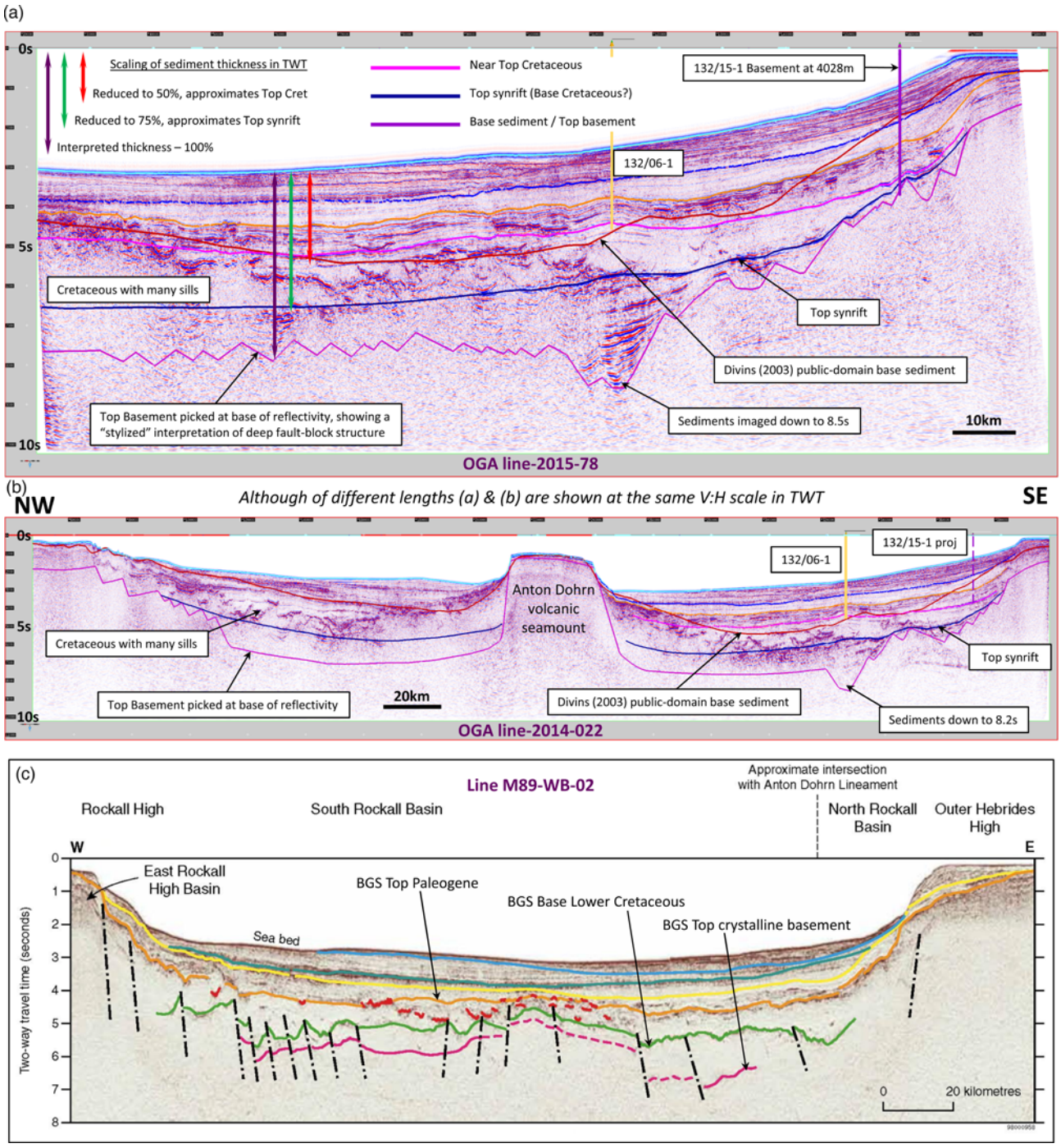

Fig. 3. (**a**) Seismic line 2015-78 from the SE UK Rockall Basin; the location is shown in Figure 2. This is the best-quality line for defining the deep structure and fill of the basin. Wells 132/15-1 (TD basement) and 132/06-1 (TD Upper Cretaceous) are located on this line. The proportional scaling of the interpreted sediment thickness, used in the modelling to address uncertainty, is illustrated. (**b**) Seismic line 2014-022 extending across the southern UK Rockall Basin; the location is shown in Figure 2. Well 132/06-1 is located on this line; 132/15-1 is projected from the north. The line is dominated visually by the post-rift Anton Dohrn Seamount in the basin centre. (**c**) BGS interpretation of line M89-WB-02, showing the interpreted base Cretaceous and top basement (adapted from Hitchen *et al.* 2013, fig. 18). The line lies *c.* 50 km south of the Anton Dohrn Seamount, close to the lines in (a) and (b), and is located accurately in Hitchen *et al.* (2013, fig. 7).

Rockall Basin, crustal-basement thickness is in the range 5–7 km, with the thinnest crustal basement in the south, thus supporting the crustal-structure model of Joppen & White (1990) in an orthogonal direction. Hauser *et al.* (1995), however, reported no seismic evidence for synrift magmatic addition in the form of underplating, which they attributed to a model of differential stretching between the upper and lower crust. England & Hobbs (1997) used the WESTLINE deep-reflection profile (England 1995) to support the general conclusions of both Joppen & White (1990) and Hauser *et al.* (1995) that crustal-basement thickness in the centre of the basin is *c.* 6 km, associated with β factors of *c.* 6. They reported that, despite the high β factors, the WESTLINE profile shows no evidence of oceanic crust or other synrift igneous activity, which they attributed to probable time-dependent extension (rather than differential stretching). More recently, Morewood *et al.* (2005) used the later-vintage RAPIDS wide-angle data to construct several transects across the central Irish Rockall Basin, the results of which support the previous general conclusion that crustal-basement thickness in the centre of the Irish Basin is *c.* 6 km, associated with β factors of *c.* 6, rising on the flanks to a thickness of *c.* 25 km.

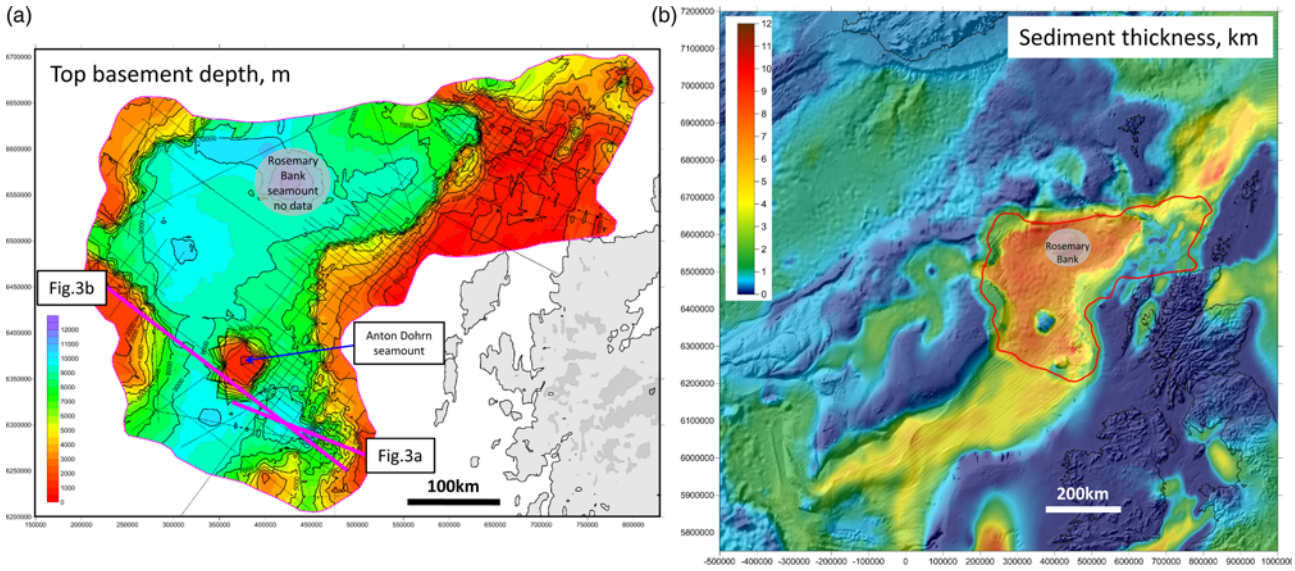

Fig. 4. (**a**) Top basement depth map (scale in metres) for the UK Rockall Basin, produced by gridding and depth-converting the interpretation in Figure 2b. The lines of the seismic grid are overlaid and the lines illustrated in Figure 3 are highlighted. (**b**) Sediment thickness (scale in kilometres) for the UK Rockall Basin (within the red polygon) merged with the regional sediment thickness for the UK–Irish Atlantic margin (Divins 2003), displayed on shaded-relief bathymetry; cf. Kimbell *et al.* (2004, fig. 6b, 2005, fig. 6) and Hitchen *et al.* (2013, fig. 16), which all use a similar colour-scaling.

In addition to the several wide-angle studies there have been other quantitative studies of the Irish Rockall Basin. Shannon *et al.* (1999) used subsidence and stretching analysis to suggest crustal β factors of *c.* 4–6, but also suggested that whole-lithosphere stretching may have been less than this. Nadin *et al.* (1999) forward-modelled Cretaceous β factors of *c.* 3, which they suggested followed a Triassic–Jurassic β factor of *c.* 1.5, giving a total β factor of *c.* 4.5. Cole & Peachey (1999), on the basis of plate reconstructions, estimated Cretaceous β factors in the range 2.2–3.75, following pre-Cretaceous stretching of magnitude *c.* 1.6. All of these results from the Irish Rockall Basin are broadly consistent with each other.

The general consensus from the previous crustal studies of the UK and Irish Rockall Basin is that, throughout the Irish sector and into the southern UK sector, crustal-basement thickness is uniformly low, in the likely range of 6–7 km, associated with β factors of *c.* 6. Further north in the UK sector, around and to the north of Rosemary Bank, crustal-basement thickness may increase to *c.* 12–13 km, associated with a reduction in β factors. It is our intention to build upon this previous work by using an interpretation of the new (2016) OGA seismic data to constrain, in more detail than previously possible, the 3D crustal structure of and stretching within the UK Rockall Basin.

Seismic interpretation of top basement

The principal aim of our interpretation of the OGA seismic data (Fig. 2) has been to define a surface for base sediment/top basement that could be used as input into both gravity-inversion and backstripping (subsidence) analyses. Within the main conclusions of their gravity-modelling study, Kimbell *et al.* (2004, p. 276) stated:

> The key to building a further generation of three-dimensional models for the NE Atlantic margin would be to focus effort on improvement of the 'initial' sediment thickness model … A key source would be regional surfaces based primarily on seismic mapping.

This captures the primary objective of our study, in terms of building upon the previous regional NE Atlantic work of Kimbell *et al.* (2004) and Kelly *et al.* (2007). The availability of the OGA seismic data provides more and better-quality seismic coverage of the UK Rockall Basin than has previously been available.

Within the area covered by the seismic data there are five wells (provided as well-ties within the seismic dataset) which penetrated top basement (Fig. 2b) (see also Hitchen *et al.* 2013, fig. 7). Three are located on the eastern flank of the Rockall Basin – 132/15-1 (Hitchen *et al.* 2013, fig. 50; Schofield *et al.* 2017, fig. 8), 154/03-1 and 164/25-2 (Hitchen *et al.* 2013, fig. 30; Schofield *et al.* 2017, fig. 9). Two are located NE of the Rockall Basin *sensu stricto*, in the area of the Rona Ridge (Fig. 1) – 202/08-1 and 205/26-1. All have been used to guide the regional interpretation, but as they all sit in structurally high flanking locations relative to the deep basin centre they do not provide any direct constraint for the interpretation of top basement in either the basin centre or on the west flank.

Figure 3a shows what is probably the best-quality seismic line within the dataset for extrapolating structures on the east flank of the basin into the basin centre. This line ties basement-well 132/15-1 (in the SE corner of the UK Rockall Tough: Fig. 2) and is also the eastern part of figure 8 in Schofield *et al.* (2017), who presumably chose to illustrate the line for similar reasons. Both Schofield *et al.* and the authors of this paper have interpreted 132/15-1 to have penetrated top basement on a west-dipping fault surface, defining a terrace on the basin flank. This is therefore a structural, rather than a base stratigraphic, tie of top basement. Top basement can be extrapolated/interpreted west from here into the basin via more fault terraces (Fig. 3a) until, below well 132/06-1 (which reached its total depth (TD) above basement, a short distance into the Upper Cretaceous), a set of bright, continuous reflections from stratigraphic fill (age unknown) are imaged at *c.* 8.5 s two-way travel time (TWT). This is the deepest clearly imaged stratigraphic fill within the basin. From older seismic data, the line drawing by Smith (2013; fig. 50 in Hitchen *et al.* 2013) suggests that these reflections are from possible intrusions within deep sediments, but Schofield *et al.* (2017, fig. 8) and the authors of this paper interpret them as coherent reflections from the sediments themselves, clearly different in seismic character to the sills higher in the section. The deep reflectivity has a downwards and westwards fanning geometry typical of fault-controlled synrift sediments. Given that we would normally expect the seismic Moho to be located at *c.* 10 s TWT (Warner 1987), i.e. at approximately the base of the seismic section, this deep reflectivity indicates that crustal basement must be thin at

this location. West of here there are indications that a set of rotated fault blocks may define top basement into the basin centre, but the 'serrated' fault-block interpretation shown in Figure 3a should be considered stylized rather than accurate.

The interpretation framework established in Figure 3a has been used to build an interpretation of top basement away from this line. Figure 3b shows the best-quality line extending across the full width of the basin, notwithstanding the presence of the Anton Dohrn volcanic seamount in the basin centre (this line is also the western part of fig. 8 in Schofield *et al.* 2017). The lines in Figure 3a and b intersect at 132/06-1, and the deep sediments below this well are again imaged in Figure 3b. Figure 3b also shows how the interpretation of top basement has been extended across to the western margin (where there are no well ties). The interpretation is guided by picking the base of any reflective package believed to be stratigraphy and by honouring the regional relationship to the better-defined higher horizons.

A number of other horizons are also shown in Figure 3. Three of these, covering the eastern part of the basin (intra-Tertiary, upper blue; top Paleocene, orange; top Cretaceous, magenta), were provided as part of the OGA dataset and provide useful constraints when interpreting the deeper structure/stratigraphy.

Figure 3a and b shows a horizon (brown) which is clearly not associated with any specific seismic event. This horizon is a TWT-conversion of the global, public-domain sediment-thickness compilation (Divins 2003). In the absence of specific information from seismic data, this is the best digital data source to use for regional studies which require sediment-thickness information. We have used it ourselves for this purpose in the past and it was used in the Rockall Basin by Kelly *et al.* (2007, fig. 6b). Figure 3 shows that the Divins public-domain top basement lies much shallower than much of the sediment fill imaged by the new seismic data and, in fact, lies close to the OGA top Cretaceous horizon. This is perhaps not a surprise, because across much of UK Rockall the extensive Paleocene volcanic cover (Ritchie & Hitchen 1996; Ritchie *et al.* 1999; Hitchen *et al.* 2013) defines an apparent seismic top basement and it is likely that the Divins compilation has been guided by the imaging of volcanics on vintage seismic data. The purpose of illustrating this horizon on the seismic data is to show how different (thicker) the sediment-thickness model derived from the new seismic data is, which in turn has a significant impact on the gravity-inversion and backstripping analyses described below.

Kimbell *et al.* (2004) also highlighted the importance of sediment-thickness information as input into gravity and backstripping models, producing their own regional sediment-thickness model as part of their study. We have, however, chosen to highlight the Divins (2003) data as the available pre-existing regional interpretation, rather than the 'optimized' sediment-thickness model of Kimbell *et al.* (2004, fig. 6b, 2005, fig. 6), for two reasons. First, the optimized Kimbell *et al.* sediment-thickness model is a product of their gravity modelling and not an input. It should therefore not be re-used as input to further gravity modelling. Second, Kimbell *et al.* (2005) stated of the input 'initial' sediment-thickness data to the Kimbell *et al.* (2004, fig. 6a) model: 'In areas where thick lavas are present, these are effectively incorporated into the crystalline component of the crustal model'. This suggests that in the northern Rockall Basin their initial base-sediment surface was probably taken at the top of the volcanics and similar to the Divins data.

The final horizon shown in Figure 3a and b (lower, dark blue) is a new interpretation, which can be carried around a number of the lines in the southern part of the OGA survey area. This is a horizon which has tentatively been picked as the top synrift, located above and younger than any observable fault extension. Not only does it lie as a capping surface above the variable-thickness sediment fill of the terraced fault blocks on the eastern margin, it also lies at the base of the thick seismically opaque Cretaceous sequence which is heavily intruded by highly reflective sills. It may therefore represent a lithological boundary above which the sills were preferentially intruded. Schofield *et al.* (2017) suggested that the sills 'preferentially exploit the mud-rich Cretaceous sequences'. In other basins around the UK, the top synrift character of this horizon would identify it as being likely to be close to the 'Base Cretaceous', and so it might be here. If so, then the fault-block structure below would be dated to the Late Jurassic (or older). There is, however, no corroborative stratigraphic evidence for this suggestion and it may equally be that this is an intra-Cretaceous horizon capping Cretaceous fault blocks. Regardless of age, where it can be interpreted, it provides a useful reference for attempting to locate/define the deeper top basement.

Figure 3c illustrates the BGS interpretation of east–west seismic line M89-WB-02 (Hitchen *et al.* 2013, fig. 18, located in their fig. 7). This line intersects our Figure 3a and b NW of well 132/06-1. The interpretation shows a 'Base Lower Cretaceous' horizon (i.e. base of the Cretaceous) some distance above a speculative 'Top crystalline basement'. The overall interpretation is not dramatically different to our own, although the Base Cretaceous and Top basement are shallower than our respective top synrift and top basement horizons. An important conclusion to draw from this line is that the northern Rockall Basin has been interpreted by the BGS to have a pre-Cretaceous structural and stratigraphic history, contrary to the suggestion of Stoker *et al.* (2017) who preferred to assign a Late Cretaceous age to the basin.

Figure 3a and b has been used to illustrate the interpretation of top basement which was carried northwards into the central area of the UK Rockall Basin, where the Paleocene volcanic cover becomes more pervasive (Ritchie & Hitchen 1996; Ritchie *et al.* 1999; Hitchen *et al.* 2013). A similar strategy for interpreting top basement was established in the northern part of the survey, where the well-tied top basement of the Rona Ridge (two wells, Fig. 2) and eastern Rockall flank (two wells, Fig. 2) was carried south and west into the central part of the Rockall Basin. This involves considerable uncertainty, but we believe the result, constrained by an interpretative geological model, provides a noticeable improvement on the previous public-domain, interpretation-based sediment-thickness information (Divins 2003; and the input model of Kimbell *et al.* 2004, fig. 6a). The completed interpretation grid for top basement, across the full extent of the OGA survey, is shown in Figure 2b.

Uncertainty in the position of top basement

The seismic interpretation of top basement (Figs 2 and 3) established an internally consistent model for the large-scale structure of the UK Rockall Basin. There are, however, considerable uncertainties in defining and picking the top basement, most particularly in the central area of the basin where pervasive Paleocene volcanics seriously impede the seismic imaging. In order to capture this uncertainty within the subsequent gravity-inversion and backstripping analyses, we have scaled the sediment thickness (in TWT) that results from the seismic interpretation (sediment thickness = top basement − bathymetry) to four percentage values: 125%, 100% (the interpreted thickness), 75% and 50%.

At 125%, top basement is placed below the interpretation on the seismic data and is considered very much a maximum likely value. At 75%, top basement is placed close to the top synrift horizon (Fig. 3a) and is therefore a likely minimum case. At 50%, top basement is placed close to both the top Cretaceous and public-domain sediment thickness (Fig. 3a), and is therefore considered to be an absolute minimum case. The gravity-inversion and backstripping analyses were both run using all four cases of sediment thickness; although the 100% interpreted case remains our preferred model.

Depth conversion

For both the gravity-inversion and backstripping analyses a map of top basement in depth is required. None of the wells drilled on the eastern flank of the Rockall Basin (Fig. 2b) provide time–depth constraints extending deep enough to be used in the undrilled (deep) central areas of the basin. We therefore opted for an external depth-conversion solution. We have used the Atlantic margins time–depth function derived and applied by Winterbourne *et al.* (2009, fig. 6a), Czarnota *et al.* (2013, fig. 3a) and Winterbourne *et al.* (2014, fig. 3a). This gives a time–depth relationship of:

$$y = 0.1136x^2 + 1.0535x$$

where y is the sediment thickness in km, and x is the sediment thickness in seconds TWT.

This function was applied to all four cases of sediment thickness in TWT and the resulting sediment-thickness isochores in depth were added to bathymetry to provide four maps of top basement in depth. Figure 4a shows the top-basement depth map for the interpreted (100%) sediment-thickness case, prepared ready for use in the backstripping analysis. Figure 4b shows the corresponding sediment-thickness map, spliced into the regional public-domain sediment-thickness map (Divins 2003) used in the gravity inversion.

A comparison of Figure 4b with Kimbell *et al.* (2004, fig. 6a) shows that our input sediment-thickness model in the UK Rockall Basin is notably thicker than the Kimbell *et al.* input model. Where their maximum input sediment thickness is uniformly in the range 4–6 km, ours is typically in the range 7–8 km and locally >8 km. The optimized sediment-thickness model of Kimbell *et al.* (2004, fig. 6b, 2005, fig. 6; Hitchen *et al.* 2013, fig. 16a), produced as a result of their gravity modelling, increased the sediment thickness from their input model into the typical range of 5–7 km, but other than in a few isolated areas their optimized model remains thinner than our interpreted input model. Interestingly, one of the areas in which their optimized model matches our own model is in the area of deep stratigraphic reflectivity below well 132/06-1 (Fig. 3a and b) (Hitchen *et al.* 2013, fig. 16a), where both models converge at sediment thicknesses of *c.* 10 km.

3D backstripping to predict basement subsidence and lithosphere thinning factors

Backstripping method and basement subsidence

The 3D backstripping and subsidence-analysis method used in this study is that of Roberts *et al.* (2013, figs 6–10), which built upon Roberts *et al.* (2009). Roberts *et al.* (2009) described the application of 3D reverse-post-rift flexural-backstripping to the case of the Norwegian Atlantic margin. Roberts *et al.* (2013) extended the technique to the analysis of synrift (Si) plus post-rift (St) subsidence (i.e. total basin subsidence) and applied this to the Campos Basin offshore Brazil. Cowie *et al.* (2015, 2016) used the same technique to investigate the subsidence of the Iberian and Angolan Atlantic margins, respectively. In the UK Rockall Basin, the objective has been to analyse the total backstripped subsidence (Si + St) of the mapped top basement (Fig. 4a).

Figure 5a shows a map of backstripped water-loaded subsidence (cf. Roberts *et al.* 2013, figs 6 and 8) for the Rockall Basin top basement (100% sediment-thickness case). This map is produced by taking the present-day basement-depth map (Fig. 4a) and removing (backstripping) all of the basin's sediment/stratigraphic fill. In so doing, a flexural-isostatic adjustment is made for the removal of the sediment load (T_e 1.5 km: Kusznir *et al.* 1995; Roberts *et al.* 1998), without a post-rift thermal correction. This produces a map of water-loaded subsidence which captures all of the synrift (Si) plus post-rift (St) subsidence experienced by the basin, without attributing any timing or magnitude to the stretching which caused the basin to develop. It is assumed that top basement was initially at sea level prior to basin subsidence. The map shown in Figure 5a has had a localized smoothing (smoothing radius 20 km) applied, so that it illustrates the regional (basin-driven) subsidence pattern without a more-local fault-controlled overprint (cf. Fig. 4a).

In order to backstrip the sediment load, the stratigraphy must be assigned a lithology. With the exception of bathymetry (available in the public domain, see Fig. 1 and Smith & Sandwell 1997; and also from the seismic data), top basement is the only horizon which has been interpreted around the full seismic survey. As a consequence, the stratigraphy has been backstripped as one unit of total-sediment-fill, to which we have assigned the lithology and compaction parameters of a shaley-sand (Sclater & Christie 1980; see also the case for the gravity inversion described below). This means that the post-rift volcanics within the basin fill have not been included as a specific lithological component with higher density. We acknowledge that this is a simplification that could ultimately be improved upon with further seismic interpretation of the Paleocene volcanic sequence. A similar simplification was made in the models of Kimbell *et al.* (2004). Although this will introduce an uncertainty into the backstripping results, we believe it to be significantly less than the uncertainty covered by the four cases of sediment thickness, which we consider to be the main uncertainty within both the backstripping and gravity-inversion analyses.

Figure 5a illustrates the backstripped subsidence from our preferred 100% sediment-thickness case. The other sediment-thickness cases are not illustrated as part of the backstripping analysis, but are included below as part of the discussion of the gravity inversion. Summarizing the (unillustrated) backstripping sensitivity to sediment thickness, where the 100% thickness model produces its maximum backstripped subsidence of *c.* 5.3 km (Fig. 5a, south-central area), the 50% case produces maximum subsidence *c.* 4.1 km, the 75% case produces maximum subsidence *c.* 4.7 km and the 125% case produces maximum subsidence *c.* 6.1 km. The effect of factoring in a denser volcanic component to the stratigraphic fill would be to reduce these values slightly.

Calculation of the lithosphere thinning factor

Maps (or profiles) of water-loaded subsidence are a direct proxy for the magnitude of lithosphere thinning factor (γ), where $\gamma = 1-(1/\beta)$ and β is the McKenzie (1978) stretching factor. Roberts *et al.* (2013, fig. 7) showed how maps of water-loaded subsidence can be converted to maps of thinning factor using either the McKenzie (1978) subsidence model directly or a modification of the McKenzie model which allows for decompression melting (magmatic addition to the crust) at high stretching/thinning factors (McKenzie & Bickle 1988; White & McKenzie 1989). In the case of the latter, as stretching proceeds beyond a given critical value the original continental crust continues to stretch and thin, but the total thickness of the crust is buffered by the addition of new magmatic material (see also Chappell & Kusznir 2008).

Figure 5b shows a map of the thinning factor for the UK Rockall Basin, derived from the subsidence map in Figure 5a. It has been produced assuming no magmatic addition at high thinning factors and is therefore a direct product of the McKenzie (1978) Si + St subsidence. Figure 5c shows the comparable map of thinning factor assuming 'normal' magmatic addition, in which magmatic addition is triggered at thinning factor 0.7 (β factor of *c.* 3.3), with a maximum magmatic addition of 7 km at thinning factor 1 (representing the generation of new oceanic crust). The other parameters incorporated into the calculation of the thinning factor for both maps are: the rift age 140 Ma (within the Early Cretaceous),

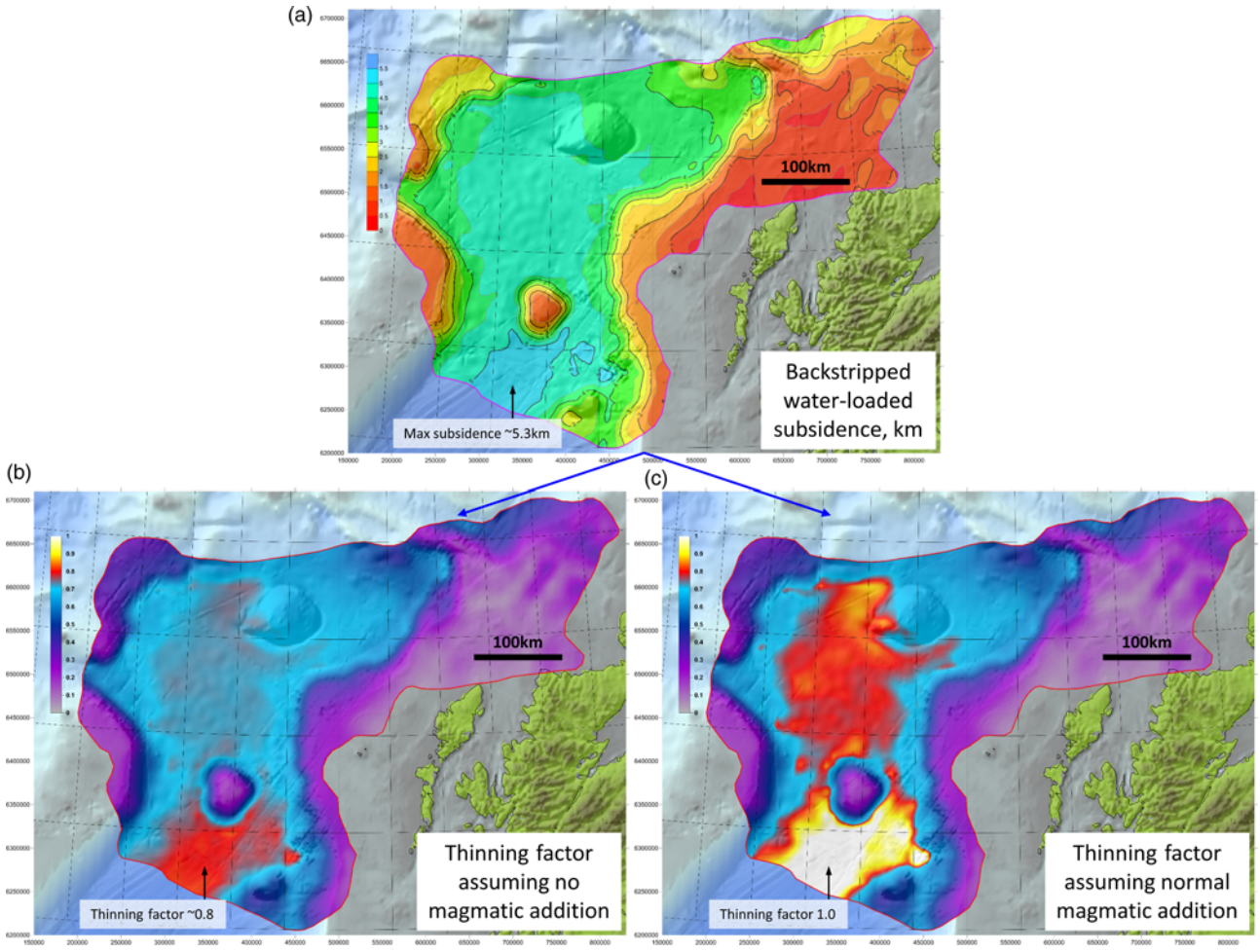

Fig. 5. (**a**) Backstripped water-loaded subsidence of the top basement (Fig. 4a) for the UK Rockall Basin (scale in kilometres). (**b**) Continental lithosphere thinning factor ($1-1/\beta$) derived from water-loaded subsidence of the basement, assuming no synrift magmatic addition. The thinning factor reaches *c.* 0.8, predicting the presence of highly thinned continental crust. (**c**) Continental lithosphere thinning factor derived from water-loaded subsidence of the basement, assuming 'normal' synrift magmatic addition (maximum of 7 km). The thinning factor reaches 1, predicting the local presence of oceanic crust which is not believed to be present. (b) is the preferred model. In (b) & (c) a rift age of 140 Ma and an initial crustal thickness of 35 km have been assumed. All maps are displayed on shaded-relief bathymetry.

the initial crustal thickness 35 km and the crustal-basement density 2850 kg m^{-3}. The same density is assumed for the magmatic addition in Figure 5c.

A restriction of the modelling techniques used in this study (subsidence analysis, gravity inversion, heat-flow prediction) is that they all require specification of a single instantaneous rift age, rather a time-dependent age range or multiple rift events. If extension is likely to have been time-dependent or punctuated, then it is sensible to choose a single rift age in the centre of the likely age range. We have chosen 140 Ma because it lies within the Early Cretaceous at the mid-point of a 40 myr range extending from 160 Ma (Oxfordian) to 120 Ma (Aptian) (see the discussion above and within Ritchie *et al.* 2013). A similar age was chosen previously for modelling the pre-break-up extension of the contiguous deep-water basins to the north, the Faeroe–Shetland Basin (Fletcher *et al.* 2013), and the Møre and Vøring basins (Roberts *et al.* 2009).

Our choice of 35 km for the initial crustal thickness corresponds with the maximum crustal thickness recorded in unstretched crust onshore Scotland (Davis *et al.* 2012, fig. 11). Ritchie *et al.* (2013, fig. 6d) used an initial crustal thickness of 30 km to map β factor from the results of Kimbell *et al.* (2004), but this value seems to be too low given that the present-day crustal thickness on the flanks of the Rockall Basin is shown to be greater than 30 km within the same set of results (Kimbell *et al.* 2005, fig. 7; Ritchie *et al.* 2013, fig. 6b).

Returning to the backstripping results, with no magmatic addition the maximum thinning factor predicted (Fig. 5b south-central area) is 0.83 (β factor of *c.* 5.9). This is consistent with the values for β of *c.* 6 reported for crustal thinning in the Irish Rockall Basin by Joppen & White (1990), Hauser *et al.* (1995), England & Hobbs (1997) and Morewood *et al.* (2005), and provides some confidence that our preferred-case mapping of top basement may be reliable. The maximum thinning factor of 0.83 implies that an initial crustal-basement thickness of 35 km will have been thinned to a present-day basement thickness of *c.* 6 km, consistent with the crustal profile from the same southern UK area produced by Keser Neish (1993). North of the Anton Dohrn Seamount (Fig. 1) axial thinning factors are lower, *c.* 0.7 (Fig. 5b), corresponding with a crustal-basement thickness of *c.* 10 km.

With magmatic addition incorporated (Fig. 5c), the maximum thinning factor predicted in the south-central area is 1. This implies that no continental-crustal basement should be present in this area and that it has been replaced by *c.* 7 km of oceanic crust. These high (oceanic) thinning factors are predicted in the area where the seismic data are of the best quality (Fig. 3). In this area we do not see any seismic evidence of oceanic crust, but rather interpret the pre-existing crustal basement to be highly extended on sets of tilted fault blocks (see also Schofield *et al.* 2017, fig. 8).

We therefore believe that the seismic data are more compatible with the non-magmatic thinning solution (Fig. 5b) than with the

magmatic case (Fig. 5c). A similar conclusion was reached by Hauser *et al.* (1995) and England & Hobbs (1997) from their analysis of the RAPIDS and WESTLINE seismic data, respectively. We share and support the conclusion by England & Hobbs (1997) that the apparent absence of synrift magmatism in areas of high stretching/thinning suggests that extension occurred over a time-dependent period rather than geologically instantaneously. Ritchie *et al.* (2013) developed this further by stating that if $\beta = 5$ then extension over a period of 10 myr or more would generate no melt. These conclusions are consistent with the suggestion that extension of the Rockall Basin occurred progressively from the Jurassic into the Cretaceous (see the discussion above).

Gravity inversion to predict crustal-basement structure and lithosphere thinning factors

Gravity-inversion method

The gravity-inversion method applied in this study follows that described in detail in several previous publications (Greenhalgh & Kusznir 2007; Alvey *et al.* 2008; Chappell & Kusznir 2008; Cowie & Kusznir 2012*a*; Roberts *et al.* 2013; Kusznir *et al.* 2018; Steinberg *et al.* 2018). It is recapped here in the specific context of the Rockall Basin.

The gravity inversion uses three principal sets of data as primary input:

- satellite free-air gravity anomaly data (Fig. 6a) (Sandwell & Smith 2009, publicly available);
- bathymetric/topographical data (Fig. 1) (Smith & Sandwell 1997, publicly available);
- sediment-thickness data, for which our interpreted sediment-thickness data for the UK Rockall Basin were embedded within the global dataset (Divins 2003), providing supporting regional context within which to run the gravity inversion (Fig. 4b). The gravity inversion is a long-wavelength calculation and works best when areas of investigation are not clipped to a local boundary and investigated in isolation.

The principal output from the gravity inversion comprises maps of:

- depth to Moho (present day);
- total crustal-basement thickness (base sediment to Moho, does not distinguish between continental and magmatic/oceanic crust);
- residual thickness of the continental crust (total crustal thickness minus predicted magmatic addition produced by synrift decompression melting);
- continental lithosphere stretching factor (β) and thinning factor (γ), where $\gamma = 1 - 1/\beta$.

Key to the success of the gravity-inversion method are two corrections made in order to account for the highly attenuated nature of the continental crust in deep-water basins and at rifted margins. They are described in detail by Chappell & Kusznir (2008), and are illustrated within the methodology workflow by Roberts *et al.* (2013, fig. 1) and Kusznir *et al.* (2018, fig. 1).

- A correction is made for the lithosphere thermal-gravity anomaly associated with the elevated geotherm produced by rifting/break-up. Because the magnitude of the gravity anomaly decreases with time as the lithosphere cools following rifting/break-up the age of rifting is important.
- A prediction can be made for magmatic addition to the crust at high stretching factors, in a similar manner to its incorporation in the water-loaded subsidence analysis (above). Following McKenzie & Bickle (1988) and White & McKenzie (1989), it is assumed that decompression melting of the lithosphere occurs at high stretching factors, resulting in magmatic addition to the total thickness of the crust (Chappell & Kusznir 2008).

Kimbell *et al.* (2004) pointed out that a problem frequently faced by gravity modelling is non-uniqueness within the solutions. They recognized (Kimbell *et al.* 2005) that, because their models sought to solve coincidently for both depth-to-Moho and depth-to-basement, there is a non-unique trade-off between the two within the results. Within our own gravity-inversion method the specification of a fixed sediment-thickness model on input and application of Smith's (1961) theorem allows for a unique solution to be obtained from any given set of model parameters.

Crustal-basement structure and lithosphere thinning factors from gravity inversion

Figure 6b–d illustrates the results of our preferred gravity-inversion model for the UK Rockall Basin. In addition to the bathymetry, sediment thickness and gravity data listed above (Figs 1, 4b and 6a), the model has been constrained by the following parameters: a rift age of 140 Ma, a density of crustal basement of 2850 kg m^{-3}, an initial crustal thickness (CT_{ini}) of 35 km and a sediment-fill lithology of shaley-sand. Each of these parameter values is shared with the subsidence analysis described above (Fig. 5). The gravity inversion is also constrained by a parameter known as the reference Moho depth (also called reference crustal thickness in some publications; see the methodology references listed at the start of the previous subsection on 'Gravity-inversion method'). The reference Moho depth (CT_{ref}) is a geophysical/geodetic parameter which represents the reference datum to which the Moho relief determined by gravity inversion is applied in order to determine the Moho depth. For the Rockall Basin, $CT_{ref} = 35$ km has been used. This is the same as the value for CT_{ini}, although there is no requirement for this to be the case. This value for CT_{ref}, which is lower than the global average value of *c.* 37.5 km, acknowledges the likely presence of *c.* 500 m of dynamic uplift in the Rockall Basin (Jones *et al.* 2002, fig. 3), which is possibly the far-field effect of the Iceland Plume (Jones *et al.* 2002). A similar correction was made within the models of Kimbell *et al.* (2004), who recognized that uplift associated with 'deep mantle effects' is holding the NE Atlantic margin shallower than would otherwise be expected.

Figure 6b shows a map of Moho depth for the UK Rockall Basin. Figure 6c shows a map of total crustal-basement thickness. Figure 6d shows a map of continental lithosphere thinning factor (cf. Fig. 5b). In the most highly stretched south-central area, the Moho rises to a minimum depth of *c.* 15 km (from an initial depth of 35 km), the minimum crustal-basement thickness is *c.* 6 km and the maximum thinning factor is *c.* 0.8 (β factor of *c.* 5). North of Anton Dohrn the axial crustal-basement thickness spans the range *c.* 6–10 km. The results shown here are for the case of no synrift magmatic addition and thus the map of total crustal-basement thickness (Fig. 6c) is also the map for the residual thickness of the continental crust. The results contained within these maps are pleasingly consistent with the previous (2D) wide-angle seismic results for crustal thickness within the UK Rockall Basin (Roberts *et al.* 1988; Keser Neish 1993; Klingelhöfer *et al.* 2005).

The maps in Figure 6 can be compared with those displaying similar results from Kimbell *et al.* (2004, 2005), which are best presented as figure 16 in Hitchen *et al.* (2013). As a general conclusion, our results show thinner crust along the deep axial region of the UK Rockall Basin and higher thinning/β factors, despite the Hitchen *et al.* (2013) map of β factor (fig. 16d) being referenced to an initial crustal thickness of 30 km (rather than 35 km used in our work). The reason why our results show greater

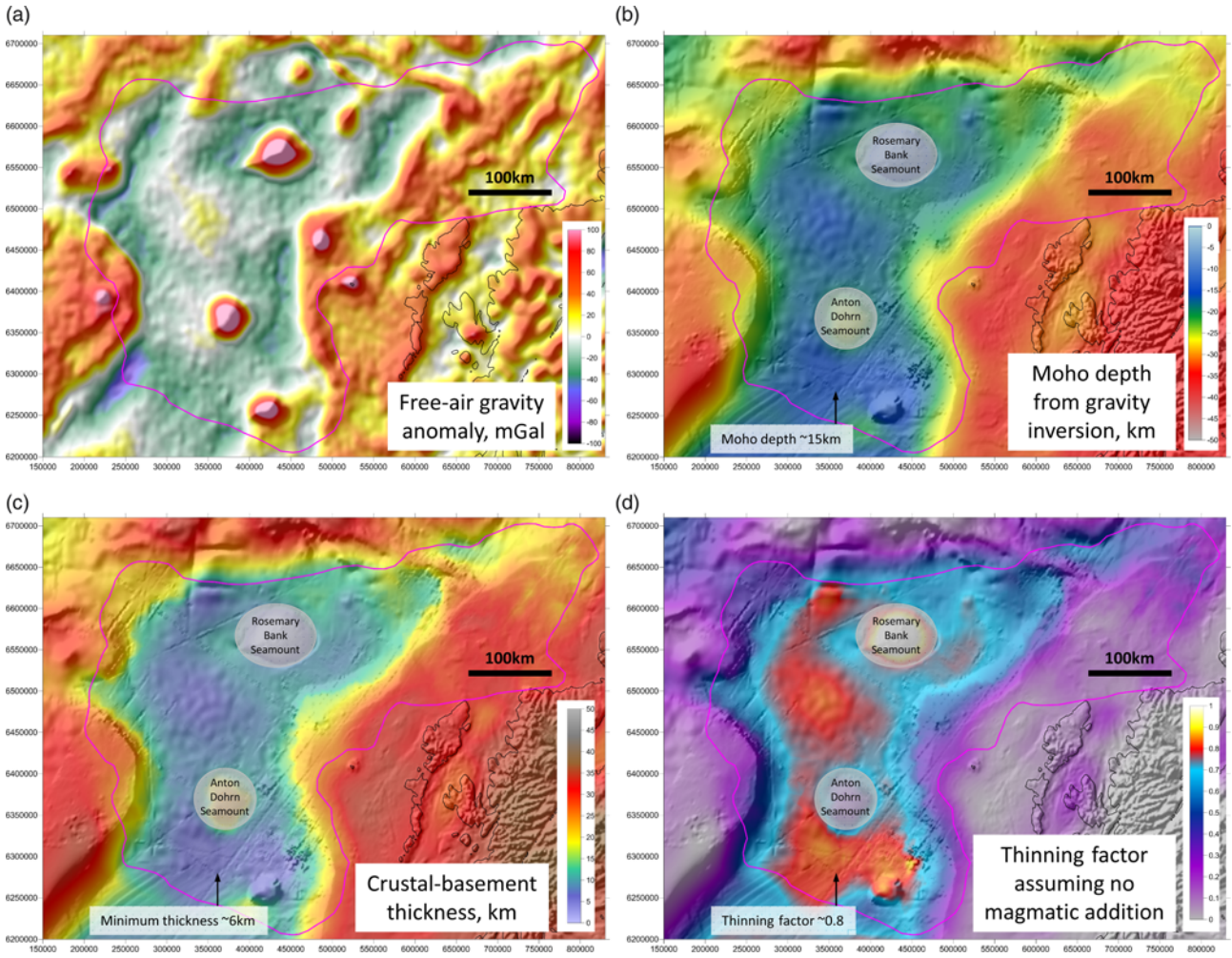

Fig. 6. Input to and results of the preferred-case gravity inversion, which uses: rift age = 140 Ma, initial crustal thickness and reference Moho depth = 35 km, no synrift magmatic addition, sediment thickness 100% case. (**a**) Satellite free-air gravity anomaly (Sandwell & Smith 2009; scale in mGal), overlain on a shaded-relief display of itself. (**b**) Moho depth (scale in kilometres). (**c**) Total crustal-basement thickness (scale in kilometres). (**d**) Continental lithosphere thinning factor ($1-1/\beta$). The thinning factor reaches *c.* 0.8, predicting the presence of highly thinned continental crust, not oceanic crust. (b)–(d) are displayed on shaded-relief bathymetry. On all maps the red polygon encloses the area of the OGA seismic dataset.

stretching and thinning of the crust is because we have used an input sediment-thickness model which is regionally thicker than the optimized sediment-thickness model of Kimbell *et al.* (2004, 2005). This in turn results in a shallower Moho from gravity modelling which, together with the deeper top basement, leads to thinner crust.

Figure 7 shows three regional, crustal cross-sections (lines 1–3) extracted from the results of the gravity inversion. Each cross-section runs along the track of a regional seismic transect (see Fig. 7 inset map): Line 2 (Fig. 7c and d) is coincident with Figure 3b; lines 1 and 2 (Fig. 7a–d) lie within what is assumed to be the basin-opening (extension) direction (NW–SE); and Line 3 (Fig. 7e and f) is a strike-line at *c.* 90° to this (SW–NE).

The cross-sections each show input bathymetry/seabed and sediment thickness/top basement, underlain by the Moho predicted by gravity inversion. The left column (Fig. 7a, c and e) shows sensitivity of Moho depth to input sediment thickness (75, 100 and 125% cases), with the preferred input and results (100% case) highlighted in solid lines. Crustal-basement thickness (Fig. 6c) is the interval between corresponding pairs of top basement and Moho depth. The right column (Fig. 7b, d and f) shows the impact of running the 100% sediment-thickness model with and without 'normal' magmatic addition (Chappell & Kusznir 2008) (cf. Fig. 5b and c). For each cross-section the assumed initial crustal thickness (CT_{ini}), prior to extension and thinning, was 35 km. Each cross-section is displayed at the same horizontal and vertical scale.

Lines 2 and 3 both cross the flank of the Anton Dohrn volcanic seamount (see inset map). Crustal-basement density within the gravity inversion is taken to be 2850 kg m^{-3} and no adjustment has been made at Anton Dohrn to accommodate possible higher (mafic intrusive) densities. An opaque mask is therefore placed over the results at Anton Dohrn to advise caution.

The three sections highlighting sensitivity to sediment thickness (Fig. 7a, c and e) show that a reduced sediment thickness results in a deeper Moho, whereas an increased sediment thickness results in a shallower Moho. For the preferred results (100% case) crustal-basement thickness in the basin centre lies in the range *c.* 6–10 km. Line 2 shows that on the basin flanks the crustal-basement thickness is >25 km. The range in sediment thickness from 75 to 125% results in the predicted Moho depth varying by *c.* 3–4 km. The results from Kimbell *et al.* (2004, 2005) and Hitchen *et al.* (2013, fig. 16) typically lie closest to our 75% case.

In the three sections which show the impact of incorporating 'normal' magmatic addition (Fig. 7b, d and f) the predicted magmatic addition is assumed to have the same density as the crustal basement (2850 kg m^{-3}) and is illustrated for graphical simplicity with an underplating geometry, although no specific magmatic-emplacement mechanism is implied. When the results with and without magmatic addition are considered, the Moho depth and total crustal thickness remain the same, as a consequence only one Moho is illustrated on each section (see also Fig. 6b and c).

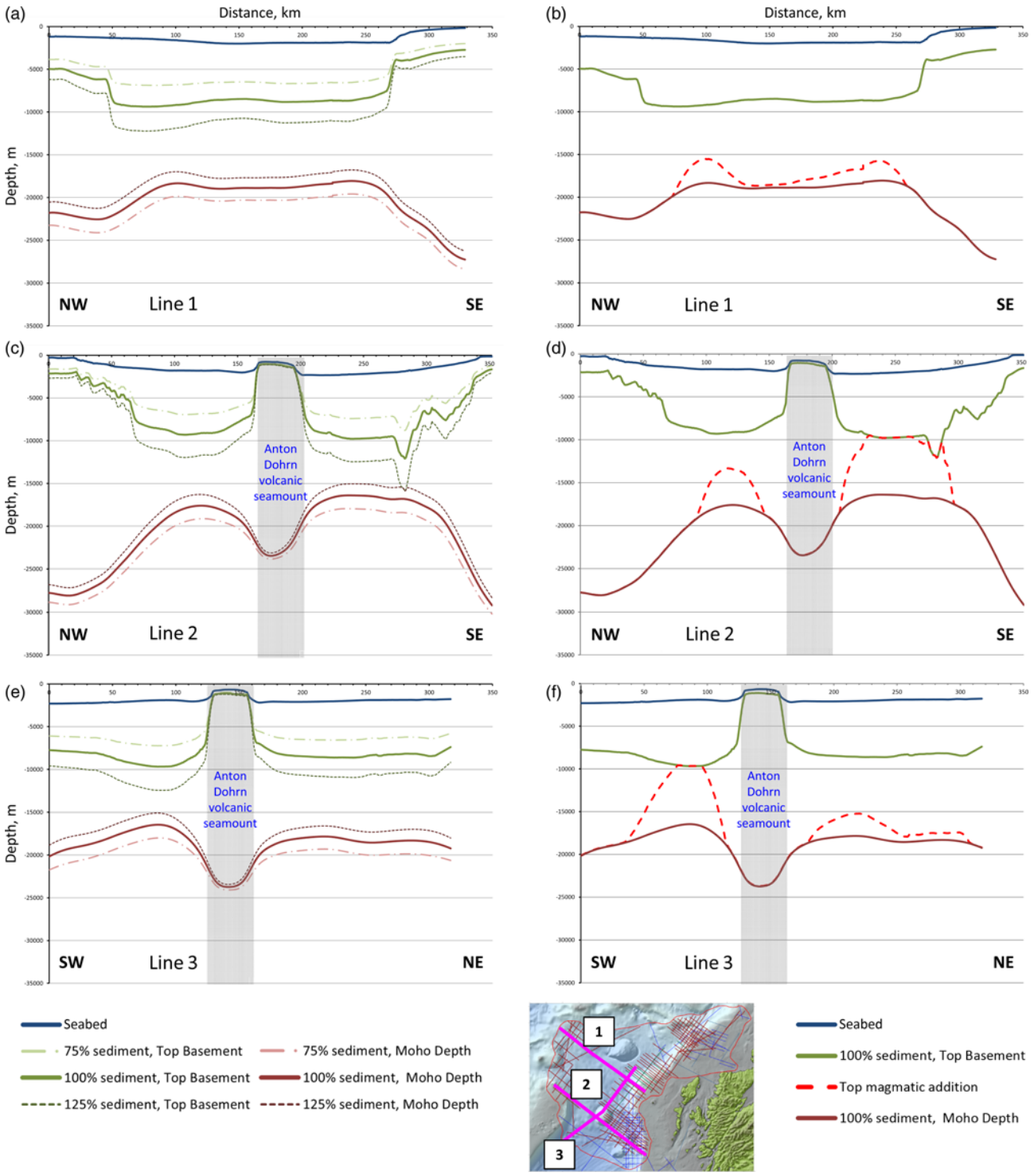

Fig. 7. Three crustal cross-sections produced from the input to and the results of the gravity inversion. The sections have been constructed along the tracks of three regional seismic transects (see the location map). (**a**), (**c**) & (**e**) highlight the sensitivity to sediment thickness, 100% is the preferred case. (**b**), (**d**) & (**f**) highlight the effects of possible synrift magmatic addition, although no magmatic addition is the preferred model. (a) Line 1, sensitivity of Moho depth to input sediment thickness. (b) Line 1, showing how 'normal' magmatic addition would impact the preferred model. (c) Line 2, sensitivity of Moho depth to input sediment thickness. (d) Line 2, showing how 'normal' magmatic addition would impact the preferred model. (e) Line 3, sensitivity of Moho depth to input sediment thickness. (f) Line 3, showing how 'normal' magmatic addition would impact the preferred model. In (b), (d) & (f) magmatic addition is illustrated for graphical simplicity with an underplating geometry.

The inclusion of magmatic addition, however, reduces the residual thickness of the continental crust (above the magmatic addition). With magmatic addition included, continental-crustal basement is locally completely replaced by magmatic addition in parts of Line 2 (SE) and Line 3 (SW). In these areas the inclusion of normal magmatic addition results in the thinning factor rising to 1 (see also Fig. 5c from the backstripping analysis), predicting the presence of oceanic crust and no continental crust. For the same reasons as discussed above (see also Hauser *et al.* 1995; England & Hobbs 1997), we prefer the non-magmatic solution in which the total crustal-basement thickness is not reduced by synrift magmatic addition.

Figure 6d shows the continental lithosphere thinning factor for the 100% sediment-thickness case and no magmatic addition.

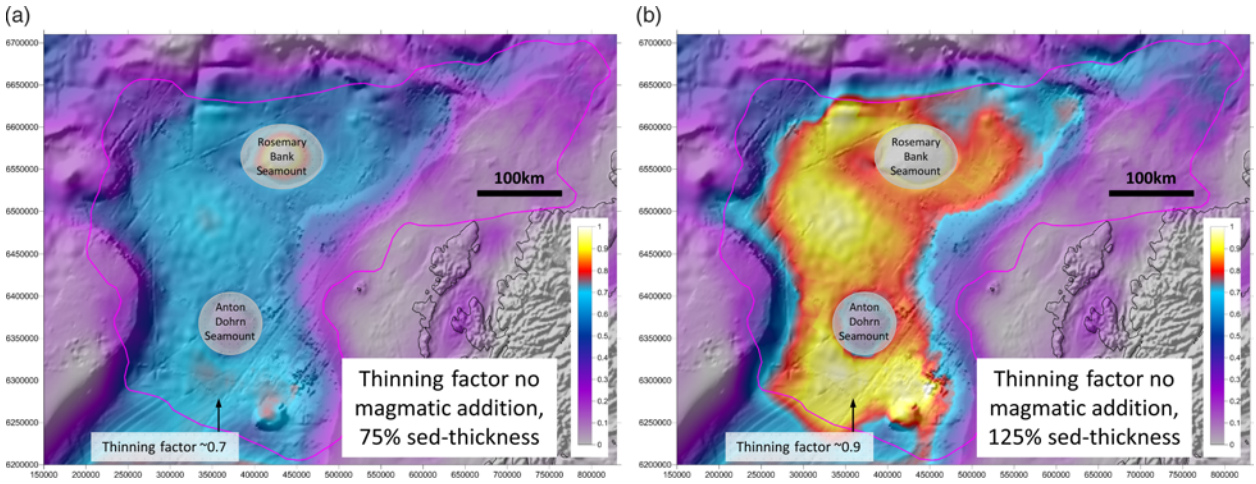

Fig. 8. Continental lithosphere thinning factor (1−1/β) from gravity inversion, for the alternative cases of (**a**) 75% sediment thickness and (**b**) 125% sediment thickness. Both maps are displayed on shaded-relief bathymetry. The red polygon encloses the area of the OGA seismic dataset. The preferred solution for the 100% sediment-thickness case is shown in Figure 6d.

Figure 8 shows the corresponding maps of the continental lithosphere thinning factor for the 75 and 125% sediment-thickness cases. These two maps cover the same sensitivity range as the cross-sections in Figure 7a, c and e. For the 75% case (Fig. 8a), the maximum thinning factor in the south-central area is *c.* 0.7. For the 125% case (Fig. 8b), the maximum thinning factor is *c.* 0.9, locally approaching 1. This is associated with a range in the minimum thickness of the crustal basement of *c.* 10 km (75% case) tending towards zero (125% case). Given the consistency of the results from our preferred 100% case with results obtained by others from the UK and Irish Rockall Basin (Roberts *et al.* 1988; Joppen & White 1990; Keser Neish 1993; Hauser *et al.* 1995; England & Hobbs 1997; Klingelhöfer *et al.* 2005; Morewood *et al.* 2005), we emphasize the preferred models illustrated in Figures 5 and 6, and have carried these results forward into the modelling of the top-basement heat-flow history described below.

The results of our preferred gravity inversion (Fig. 6) compare very well with the results of our preferred backstripping model (Fig. 5). This is one of the principal reasons for running both analyses in parallel. The backstripping and gravity-inversion methods involve different calculations aimed at producing the same general set of results which define the crustal-basement structure. If the same common parameter set is adopted for each model then the results should be similar (as they are here), providing confidence that, for the assumptions made, the results are reliable.

Our results for crustal thickness and thinning factor from both backstripping and gravity inversion do not take into account the possibility of crustal thickening by magmatic underplating, associated with the extensive post-rift Tertiary volcanism seen within the Rockall Basin (see the discussion by Clift & Turner 1998). This hypothesis was tested quite rigorously by Klingelhöfer *et al.* (2005), who concluded that, although there is probably Tertiary underplating at the Atlantic margin to the west, no evidence for underplating could be found below the Rockall Basin. We therefore believe that no magmatic addition correction is required.

Predicting the rift-related top-basement heat-flow history from the results of the gravity inversion

Cowie & Kusznir (2012*b*) outlined a method for converting thinning-factor and crustal-thickness results from gravity inversion into predictions of present-day top-basement heat flow, applying this to the case of the Eastern Mediterranean. Here we will use and expand upon this method for the UK Rockall Basin.

Top-basement heat flow within a rift basin or continental margin results primarily from a combination of three heat sources:

(1) Radiogenic heat input from the underlying continental basement, which, following rifting, is thinned from its initial pre-rift thickness.

(2) Heat input from the transient elevated geotherm which results from lithosphere stretching and thinning, the relaxation of which results in post-rift thermal subsidence.

(3) Long-term, steady-state, heat loss from the mantle (*c.* 30 mW m^{-2}) (e.g. McKenzie 1978; Sclater *et al.* 1980; Vitorello & Pollack 1980).

Information about the continental crustal-basement thickness (e.g. Fig. 6c) allows us to put constraints on the radiogenic heat input – (1) above – which (long-term radioactive cooling notwithstanding) is constant with time following rifting and crustal thinning. Information about the thinning factor and rift age (e.g. Fig. 6d) allows us to constrain the transient heat input – (2) above – which will vary with time as a consequence of post-rift cooling. Adding all three components together gives the total top-basement heat flow into the basin at any given time.

Once the rift age and thinning factor are known, the transient heat flow can be calculated (McKenzie 1978). The radiogenic heat flow, however, is not only dependent on the thickness of the crustal basement but also on its radiogenic properties, which can be highly variable and dependent on basement lithology. For example, granitic crust will be much more radiogenic than quartzitic crust. A global average value for radiogenic heat productivity from unthinned continental crust is *c.* 30 mW m^{-2} (e.g. Vitorello & Pollack 1980). This is the value used by Cowie & Kusznir (2012*b*) for their work in the Mediterranean. Without direct measurements from the basement or reliable downhole temperature data, however, neither of which is available for the UK Rockall Basin, we cannot calibrate crustal radiogenic heat productivity to a specific value. In order to capture a realistic range of possibilities, therefore, we have calculated heat-flow models for three cases of initial crustal radiogenic heat productivity, 15, 30 and 45 mW m^{-2}, which cover the range 50–150% of the global average value.

Figures 9 and 10a show maps of predicted top-basement heat flow for the UK Rockall Basin. They are derived from the results of the preferred-case gravity inversion (Fig. 6 and the discussion above). These maps show heat flow into the basin from the basement, without the effects of sediment blanketing: that is, they represent heat flow into a water-filled basin. For a full petroleum-systems analysis, the

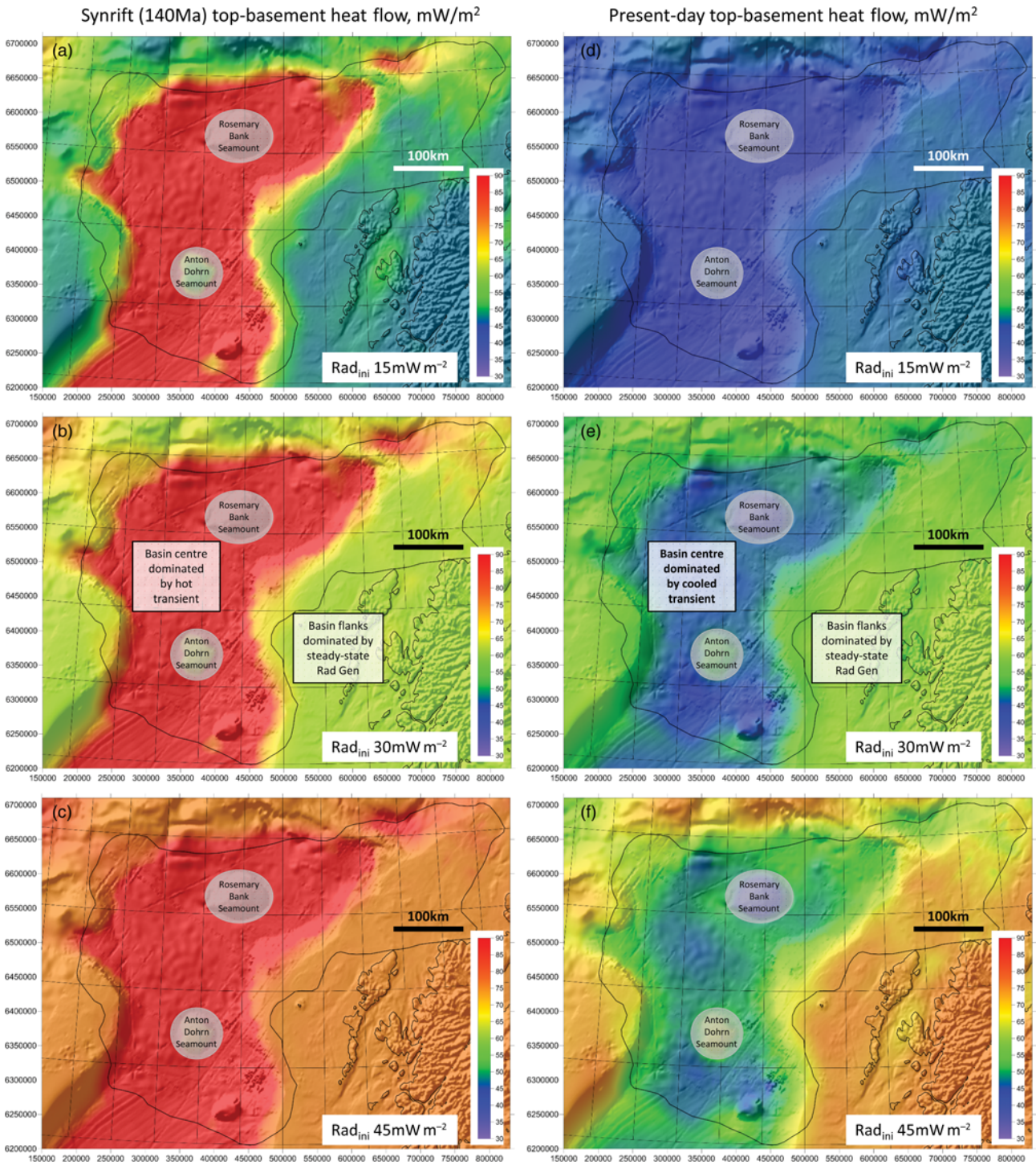

Fig. 9. Top basement heat flow for the UK Rockall Basin (scale in mW m^{-2}), derived from the gravity-inversion results in Figure 6. (**a**)–(**c**) Synrift (140 Ma) and (**d**)–(**f**) present day. (a) Synrift heat flow for initial crustal radiogenic heat productivity (Rad_{ini}) = 15 mW m^{-2}. (b) Synrift heat flow, Rad_{ini} = 30 mW m^{-2}. (c) Synrift heat flow, Rad_{ini} = 45 mW m^{-2}. (d) Present-day heat flow, Rad_{ini} = 15 mW m^{-2}. (e) Present-day heat flow, Rad_{ini} = 30 mW m^{-2}. (f) Present-day heat flow, Rad_{ini} = 45 mW m^{-2}. Predicted heat flow does not include the effects of sediment blanketing.

additional effects of sediment blanketing should be incorporated. Note that for uniformity of scale and optimum dynamic range across all maps in Figures 9 and 10a, the heat-flow colour map has been clipped at 90 mW m^{-2}, although some maps contain values above this limiting value.

Figure 9a–c shows predicted synrift (in our model 140 Ma, Early Cretaceous, see the discussion above) top-basement heat flow for the three cases of initial crustal radiogenic heat productivity, 15, 30 and 45 mW m^{-2}. In all three cases the central, deep-water Rockall Basin shows high heat-flow values dominated by the transient component resulting from high thinning factors (Fig. 5b and 6d). The synrift heat flow across the central Rockall Basin lies in the range 100–200 mW m^{-2} for all three cases and because of the dominance of the transient component there is no significant variation at any given location in the basin centre between the three models. Note that the synrift heat flow is mapped onto the present-day, post-rift geometry of the basin, attained upon completion of all extension, probably during the Early Cretaceous. The maps therefore represent the distribution of heat flow upon completion of extension, within the constraints of the instantaneous stretching model which we have applied.

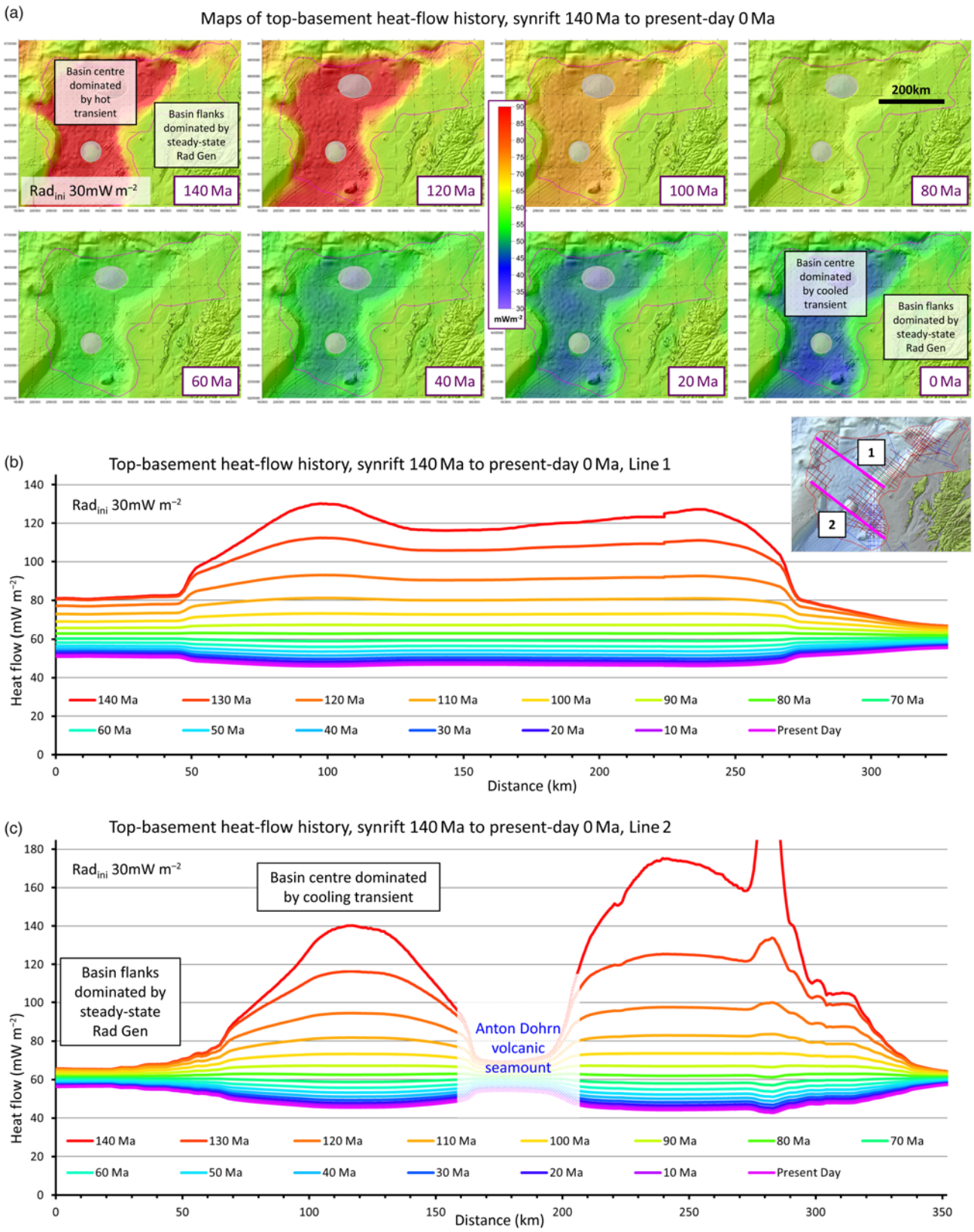

Fig. 10. (**a**) Maps of top-basement heat flow (scale in mW m^{-2}), showing the full history from synrift (140 Ma) to present day, at increments of 20 myr. Initial crustal radiogenic heat productivity (Rad$_{ini}$) = 30 mW m^{-2}. Note how in the highly stretched basin centre the heat flow changes significantly over time, whereas on the less-stretched basin flanks changes with time are much reduced. (**b**) & (**c**) Profiles of heat-flow history for the same model as (a), at increments of 10 myr, along lines 1 and 2 (see the inset map for the location; see also Fig. 7).

On the less highly stretched basin flanks there is a more noticeable difference in the synrift heat flow between the three models (Fig. 9a–c), covering a range of *c.* 20 mW m^{-2} at any given location. On the basin flanks, heat flow is controlled more by the radiogenic heat input from the basement and less by the transient component. With thicker crustal basement preserved on the basin flanks the variation in the initial radiogenic component becomes more significant than it is in the highly thinned basin centre.

Figure 9d–f shows the predicted present-day top-basement heat flow for the same three models as Figure 9a–c. In the deep-water

basin centre the high synrift transient component has largely relaxed after 140 Ma, and the heat flow is low in all three cases. With the transient component reduced to *c.* 10% of its initial value, the effect of the variable radiogenic heat input from the remaining thin crust results in a visible difference between the three models, covering the range *c.* 40–50 mW m^{-2} in the basin centre. At the synrift stage (Fig. 9a–c) heat flow in the basin centre is far higher than it is on the basin flanks, whereas at the present day (Fig. 9d and e) heat flow in the basin centre is lower than it is on the flanks.

On the basin flanks the present-day heat flow is again controlled predominantly by the radiogenic input from the crust (Fig. 9d–f), plus the long-term steady-state heat loss from the mantle. Present-day heat flow on the flanks is less than at the synrift stage, but much less significantly so than in the basin centre. The initial transient component was relatively low on the basin flanks and consequently the result of its cooling has a much reduced impact.

Figure 10a shows the full heat-flow history, at 20 myr increments, for the heat-flow model with an initial crustal radiogenic heat input of 30 mW m^{-2}. The history begins at the synrift stage (140 Ma; see also Fig. 9b) and ends at the present day (see also Fig. 9e). The maps of heat-flow history demonstrate clearly the different thermal evolution of the basin centre and the basin flanks. The basin centre is dominated by the heat-flow change related to the cooling of the high synrift thermal transient. On the basin flanks the heat-flow change is much more subtle, with little change over time in these areas of lower stretching/thinning. Note that at 80 Ma the top-basement heat flow is approximately uniform across both the basin centre and the flanks. This is a consequence of the basin centre cooling from hotter than the flanks to cooler than the flanks over time.

Figure 10b and c shows the same heat-flow history as Figure 10a, but in 2D-profile format at increments of 10 myr. Figure 10b shows the heat-flow history for Line 1 (Fig. 7a and b) and Figure 10c shows the heat-flow history for Line 2 (Fig. 7c and d, see also Fig. 3b). The presence of the Anton Dohrn volcanic seamount on Line 2 perturbs the heat-flow calculations in the centre of the line, because the gravity inversion cannot correctly calculate the lithosphere thinning factor here (Fig. 6d). An opaque mask is therefore placed over the results at Anton Dohrn, and the heat-flow results here and in the immediately adjacent areas should not be used.

The 2D plots again show clearly how the highly stretched basin centre cools over time, from initially substantially hotter (120–180 mW m^{-2}) than the basin margins to cooler than the basin margins at the present day (*c.* 45 mW m^{-2}). The green curves at 80–70 Ma capture the time at which heat flow into the basin was approximately uniform across both the flanks and the basin centre (*c.* 60 mW m^{-2}).

At the basin margins, particularly on Line 2 (Fig. 10c), there is little variation in heat flow through time. The initial transient heat flow at the basin margins was not large and heat flow in these areas is dominated by the constant crustal-radiogenic component, plus the long-term steady-state heat loss from the mantle.

Additional considerations outwith the heat-flow models

The models of top-basement heat flow presented in Figures 9 and 10 specifically address the impact of the major stretching event which created the Rockall Basin. There are a number of other geological factors which might be considered to have influenced the heat-flow history but which are not incorporated into our models. These are discussed briefly here.

Tertiary break-up-related stretching

The Atlantic margin west of the Rockall Basin (Fig. 1) formed by continental break-up at *c.* 55 Ma (e.g. White *et al.* 2010). There are no visible signs of any break-up-related extension (i.e. faulting) within the Rockall Basin and at its closest the NW corner of the UK Rockall Basin still lies *c.* 200 km east of the Atlantic continental margin (Fig. 1). Previous modelling work on the Norwegian Atlantic margin (e.g. Roberts *et al.* 1997, 2009; Kusznir *et al.* 2005) has shown that lithosphere-scale stretching related to break-up probably extends a maximum of *c.* 200 km inboard of the ocean margin and generally less than this. It is therefore unlikely that lithosphere-scale stretching associated with Atlantic break-up has affected the heat-flow history of the Rockall Basin.

Early Tertiary dynamic uplift

Transient Paleocene dynamic uplift of the North Sea and Faeroe–Shetland basins was quantified by Nadin & Kusznir (1995) and Nadin *et al.* (1995, 1997), who also showed that this dynamic support was withdrawn during the Eocene, causing accelerated Eocene subsidence of these basins. Jones *et al.* (2002) suggested that this transient uplift extended as far south as the Porcupine Basin (south of the Rockall Basin, offshore Ireland) and by implication therefore transient Paleocene uplift is likely to have also affected the Rockall Basin. Discussion within Hitchen *et al.* (2013) supports this view. Nadin *et al.* (1995, 1997) and Jones *et al.* (2002) attributed the transient uplift to dynamic mantle support around the Iceland Plume at the time of continental break-up. They did not consider it likely to be a lithosphere-scale thermal event because the time duration of the uplift (*c.* 10 myr) was too short. It is unlikely therefore that transient Paleocene uplift followed by Eocene subsidence had an impact on the basement heat-flow history in any of these basins, including the Rockall Basin.

Tertiary compression

Tertiary compressional structures around the margins of the Rockall Basin have been documented by Tuitt *et al.* (2010) and Kimbell *et al.* (2017). Compressional structures have not, however, been recorded within the Rockall Basin itself and therefore it is unlikely that there was any crustal-basement thickening and associated heat-flow perturbation within the basin during the Tertiary. In addition, where similar Tertiary compressional structures have been studied quantitatively offshore Norway (Roberts *et al.* 2009; see also Kimbell *et al.* 2017), their tectonic signature has been shown to be a very minor folding strain amplified significantly by subsequent differential sediment loading (e.g. Stuevold *et al.* 1992). Their likely lithosphere-scale effect on basement heat-flow would consequently be close to zero.

Tertiary magmatic activity

This is potentially the most significant omission from our heat-flow models. The presence of major volcanic features such as Anton Dohrn and Rosemary Bank, plus the pervasive nature of the post-rift early Tertiary lavas, clearly indicate some form of thermal perturbation within the Rockall Basin during the early Tertiary. We have discounted above the thermal impact of lithosphere-scale stretching and dynamic uplift at this time, while Klingelhöfer *et al.* (2005) concluded that there was no regional magmatic underplating associated with the presence of the overlying volcanic features. It seems likely therefore that the primary impact of Tertiary magmatism on heat flow within the Rockall Basin would have been intense local heating associated with the introduction of magmatic material through the crust and into the basin fill. While acknowledging that this is likely to have occurred, we are unable to incorporate these geographically or stratigraphically focused events into our regional models of rift-related heat flow from within the basement.

In a recent study focused specifically on the thermal structure of volcanic margins, Armitage & Collier (2017) also concluded that they could not estimate the heat-flow anomaly resulting from the addition of heat by crustal intrusions, in the North Atlantic and elsewhere. They did, however, identify that thermal perturbation resulting from local melt intrusion was likely to have a relatively short time duration of *c.* 1 myr, approximately two orders of magnitude less than the duration of the lithosphere-scale thermal perturbation resulting from rifting/break-up (e.g. Figs 9 and 10). The impact of Tertiary magmatic activity on our long-term heat-flow predictions is therefore likely to have been minimal and our results are considered to be robust at the regional scale for which they are intended.

The UK Rockall Basin in its regional context on the Atlantic margin

Finally, we will look at the crustal structure of the UK Rockall Basin within the regional context of the UK/Irish Atlantic margin. Figure 11a shows a regional map of crustal-basement thickness for the UK/Irish Atlantic margin, which covers the full extent of the Rockall Basin. This map was produced using the same parameters as our preferred case gravity inversion (Fig. 6: rift age of 140 Ma, no magmatic addition, CT_{ini} of 35 km and CT_{ref} of 35 km), except that all sediment-thickness information is public domain (Divins 2003). Figure 11b shows the corresponding map of the continental lithosphere thinning factor. In the central, deep-water Irish Rockall Basin crustal thickness is in the range *c.* 4–7 km with corresponding thinning factors of 0.8 or greater (β factor of *c.* 5 or greater). These results are consistent with the results or conclusions of previous work in this area (Joppen & White 1990; Hauser *et al.* 1995; England & Hobbs 1997; Morewood *et al.* 2005). Close to the boundary between the Irish and UK sectors of the Rockall Basin, Figure 11a and b suggests that there is a significant change to the crustal structure of the basin, with crustal thickness in the UK sector mapped at *c.* 15 km and the thinning factor in the range *c.* 0.5–0.6. A similar change in regional crustal thickness between the Irish and UK sectors of the Rockall Basin is apparent in the models of Kimbell *et al.* (2004, 2005; also Hitchen *et al.* 2013, fig. 16) and Kelly *et al.* (2007).

When we first produced these results (Fig. 11a and b), prior to working with the OGA seismic data, we believed that this northwards increase in crustal-basement thickness probably represented a genuine northwards reduction in extension and thinning within the Rockall Basin. Having worked with the OGA data, however, we have revised this opinion. Figure 11c and d shows the corresponding maps of crustal-basement thickness and thinning factor produced by splicing our new top-basement/sediment-thickness model (Fig. 4) into the regional gravity inversion. The updated results show a continuity of crustal thickness and thinning factor along the full length of the Rockall Basin, producing what we believe is a more reliable regional result, compatible with previous 2D crustal-structure modelling in the basin (Roberts *et al.* 1988; Joppen & White 1990; Keser Neish 1993; Hauser *et al.* 1995; England & Hobbs 1997; Klingelhöfer *et al.* 2005; Morewood *et al.* 2005). As discussed above, we believe that the difference between the two models results from the public-domain sediment thickness extending down only to the approximate level of the Paleocene volcanics in the UK Rockall Basin. Our new sediment-thickness model, based on the OGA seismic data, is believed approximately to double the sediment thickness within the basin centre. It is for similar reasons that the models of Kimbell *et al.* (2004, 2005; also Hitchen *et al.* 2013) and Kelly *et al.* (2007) show a similar apparent change in crustal structure. Kelly *et al.* (2007) used the same public-domain sediment-thickness information (Divins 2003) for all of the Rockall Basin as used in our Figure 11a and b, and the resulting crustal model is therefore very similar. Kimbell *et al.* (2004, fig. 6a) used a different (proprietary) sediment-thickness model to the Divins (2003) data, but it was still one in which input base sediment was apparently taken at top volcanics (Kimbell *et al.* 2005) and then modified during the gravity modelling. The resulting optimized sediment thickness (Kimbell *et al.* 2004, fig. 6b; Hitchen *et al.* 2013, fig. 16a) is still thinner than our sediment-thickness model interpreted from the OGA seismic data. For this reason, although the change in crustal structure illustrated by Kimbell *et al.* (2005) and Hitchen *et al.* (2013) is less than that in our Figure 11a and b, it is still present in the results of their gravity modelling

In Figure 11c and d the thick crust of Hatton Bank almost defines an isolated microcontinental block, bounded to the NW by the Tertiary Atlantic Ocean and to the SE by the older Rockall Basin. The two margins to Hatton Bank are probably *c.* 80 myr apart in age and are not related to the same episode of rifting/break-up. Figure 11c and d also helps to illustrate the likely continuity of extension within the Rockall Basin further to the NE into the Faeroe–Shetland Basin (Fletcher *et al.* 2013), from where it continues further to the NE into the Norwegian Atlantic margin (Lundin & Doré 2011).

The Anton Dohrn Lineament

Kimbell *et al.* (2005, figs 6 and 7) used the results from Kimbell *et al.* (2004) to identify a feature which they named the Anton Dohrn Lineament; also illustrated and discussed within Hitchen *et al.* (2013, figs 7 and 16), and discussed by Stoker *et al.* (2017). The Anton Dohrn Lineament is a broad (*c.* 100 km-wide) NW–SE-striking zone which passes through the Anton Dohrn Seamount (Fig. 1). There is no discrete fault associated with the Anton Dohrn Lineament (see Fig. 3c as an example of this), although it is itself shown in map form to comprise 'a group of three lineaments' (Kimbell *et al.* 2005).

The Anton Dohrn Lineament is identified from its association with a number of different geological features (Kimbell *et al.* 2005; Hitchen *et al.* 2013). At depth, it may separate two different Precambrian basement provinces known to be present onshore in Scotland (Dickin 1992). It coincides with an offset in the axis of the Rockall Basin, helping to define the south (Irish) and north (UK) basins. It marks an alignment in volcanic features on Hatton Bank, west of the Rockall Basin. Finally, it is believed to mark a difference in crustal structure and sediment thickness between the south and north Rockall basins, as identified from the gravity-modelling results of Kimbell *et al.* (2004). We believe, however, that the integration of our new sediment-thickness model for north Rockall into our regional gravity inversion (Fig. 11c and d) casts doubt on the latter, as these maps show continuity of crustal-basement structure and basin stretching along the full Irish–UK extent of the Rockall Basin. If the Anton Dohrn Lineament exists, therefore, it appears that it does not fundamentally partition crustal structure and basin fill on either side.

We are not, however, seeking to dismiss the Anton Dohrn Lineament in its other manifestations. Although outside the scope of this study, we accept that there may be a change in basement type and volcanic alignment along the lineament, and that these features may give rise to its magnetic expression (Kimbell *et al.* 2005, fig. 2). We are also comfortable that it coincides with an offset in the basin axis as a kinematic transfer zone, as originally suggested by Kimbell *et al.* (2005). It is worth, however, reiterating the point made by Kimbell *et al.* (2005, p. 943) that 'the transform model does not require strike-slip movements within the continental basement': that is, it is a zone of distributed displacement transfer within the network of basin-bounding faults and not itself a discrete fault structure.

Summary and conclusions

We have interpreted top basement/base sediment around the full extent of the publicly available OGA seismic dataset for the UK

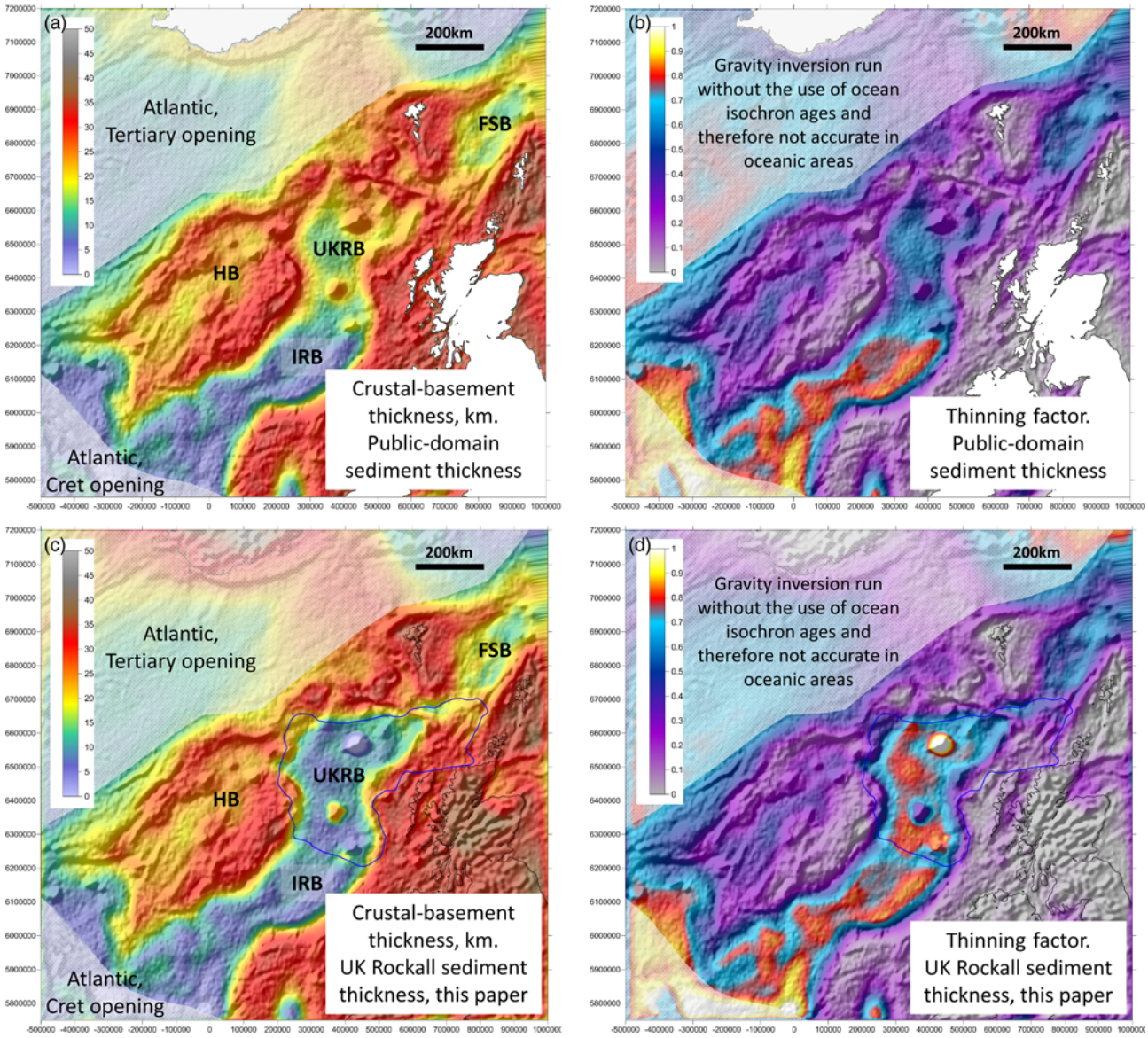

Fig. 11. Results from two regional gravity-inversion models for the UK–Irish Atlantic margin: (**a**) & (**b**) have used public-domain sediment-thickness data (Divins 2003); and (**c**) & (**d**) have used the new sediment-thickness data for the UK Rockall Basin (inside the blue polygon), merged with the public-domain data elsewhere. All other parameters and input are as in Figure 6. (a) Crustal basement thickness (scale in kilometres). (b) Continental lithosphere thinning factor. (c) Crustal basement thickness (scale in kilometres). (d) Continental lithosphere thinning factor. UKRB, UK Rockall Basin; IRB, Irish Rockall Basin; HB, Hatton Bank; FSB, Faeroe–Shetland Basin. The gravity inversions have been run without the use of ocean isochron ages to constrain the oceanic thermal-gravity anomaly (a rift age 140 Ma is used everywhere). As a consequence, the results for Atlantic oceanic crust are not accurate and are masked.

Rockall Basin (Fig. 2). This has produced a new model for the thickness of the sediment/stratigraphic fill within the basin (Fig. 4), which is substantially thicker than previously available public-domain data (Divins 2003), and also thicker than both the input data and output model of Kimbell *et al.* (2004).

The new sediment-thickness model has been incorporated into a 3D backstripping study, which has produced maps of subsidence and thinning factor across the UK Rockall Basin (Fig. 5). Analysis of backstripped subsidence shows the thinning factor reaching peak values of *c.* 0.8–0.85 (β factor of *c.* 6) in the south-central part of the UK Rockall Basin, reducing in value to *c.* 0.7 north of Anton Dohrn Seamount.

The new sediment-thickness model has also been incorporated into a 3D gravity-inversion study, mapping Moho depth, crustal thickness and thinning/stretching factor for the UK Rockall Basin (Figs 6 and 7). The results show that the crustal-basement thickness has been reduced to *c.* 6 km in the south-central area of maximum thinning, spanning the range of *c.* 6–10 km in the axial region north of Anton Dohrn. The results of the best-case backstripping and gravity-inversion analyses are consistent with each other, providing corroboration of their reliability for our chosen parameter set. The results of both studies are also consistent with previous wide-angle and deep-seismic studies of crustal structure in the Rockall Basin (Roberts *et al.* 1988; Joppen & White 1990; Keser Neish 1993; Hauser *et al.* 1995; England & Hobbs 1997; Klingelhöfer *et al.* 2005; Morewood *et al.* 2005).

The results from the best-case gravity-inversion model have been used to make predictions about rift-related top-basement heat-flow history for the UK Rockall Basin (Figs 9 and 10). Heat flow in the basin centre is shown to have been highly variable (and reducing) over time, associated with the cooling of the initially high synrift transient heat-flow component. On the basin flanks heat flow was

probably less variable over time, with its magnitude controlled primarily by constant radiogenic heat input from the basement, rather than by the transient geotherm anomaly. It is hoped that the mapping of potential heat flow into the basin will provide a useful framework for future petroleum-systems studies in the area.

Although we have identified what we believe to be the best-case parameter set for each part of the study, there are considerable uncertainties associated with our interpretation and analysis. We identified these during the study and have attempted to address them with appropriate sensitivity analyses:

- Sediment thickness interpreted on the seismic data is considered to be the most significant uncertainty. We have addressed this by running backstripping and gravity-inversion (Figs 7 and 8) models using 125, 100, 75 and 50% of the interpreted TWT thickness.
- With little relevant well data available, rift age within the Rockall Basin has not yet been definitively identified. We have addressed this by choosing a rift age of 140 Ma, which is within the Early Cretaceous and represents a median value to a possible range which might span *c.* 160–120 Ma.
- Our lithology model for the sediment/stratigraphic fill has not included a volcanic component because the thickness of the Paleocene volcanics has not been interpreted or mapped. Our density model for the bulk sediment fill in both the backstripping and the gravity inversion may therefore be a slight underestimate.
- Both the backstripping and gravity-inversion models can incorporate magmatic addition associated with high stretching/thinning factors (Figs 5 and 7). We have opted for a non-magmatic model as our preferred case (perhaps the consequence of time-dependent extension) because we see no seismic evidence that igneous activity accompanied Jurassic–Cretaceous rifting (see also England & Hobbs 1997). The Paleocene volcanics, sills and seamounts/volcanoes are all associated with post-rift volcanism, unrelated to the opening of the basin.
- The major uncertainty within the heat-flow modelling is constraining the magnitude of crustal radiogenic heat input from the basement. We have addressed this by assuming three initial values for unstretched/unthinned basement: 15, 30 and 45 mW m^{-2} (Fig. 9). These values are based on the global average value of 30 mW $m^{-2} \pm 50\%$.

When a regional gravity-inversion model is run, using our new sediment-thickness model for the UK Rockall Basin spliced into regional public-domain sediment-thickness information, we find that structural and stretching continuity at the crustal scale is mapped along the full length of the UK–Irish Rockall Basin (Fig. 11).

Acknowledgements We thank the OGA for making the Rockall Basin seismic data available for free public use, under the licence attribution: © Crown Copyright. Contains public sector information licensed under the Open Government Licence v3.0. The four reviewers, Richard England, Tony Doré, Martyn Stoker and Peter Dromgoole, are thanked for pointing out the errors and, particularly, the omissions in our original manuscript. Our colleagues Graham Yielding, Dave Quinn and Amy Clarke are thanked for help with setting up the seismic interpretation project in TrapTester™. We thank Iain Scotchman for editorial feedback on the final version of the manuscript.

Funding We thank the OGA for funding an initial 2D pilot study as part of the 2016 Exploration Licence Competition. The subsequent 3D study, from which this publication derives, was internally funded by Badley Geoscience.

References

Alvey, A., Gaina, C., Kusznir, N.J. & Torsvik, T.H. 2008. Integrated crustal thickness mapping and plate reconstructions for the high Arctic. *Earth and Planetary Science Letters*, **274**, 310–321, https://doi.org/10.1016/j.epsl.2008.07.036

Archer, S.G., Bergman, S.C., Iliffe, J., Murphy, C.M. & Thornton, M. 2005. Palaeogene igneous rocks reveal new insights into the geodynamic evolution and petroleum potential of the Rockall Trough, NE Atlantic Margin. *Basin Research*, **17**, 171–201.

Armitage, J.J. & Collier, J.S. 2017. The thermal structure of volcanic passive margins. *Petroleum Geoscience*, first published online November 23, 2017, https://doi.org/10.1144/petgeo2016-101

Chappell, A.R. & Kusznir, N.J. 2008. Three-dimensional gravity inversion for Moho depth at rifted continental margins incorporating a lithosphere thermal gravity anomaly correction. *Geophysical Journal International*, **174**, 1–13.

Clift, P.D. & Turner, J. 1998. Paleogene igneous underplating and subsidence anomalies in the Rockall–Faeroe–Shetland area. *Marine and Petroleum Geology*, **15**, 223–243.

Cole, J.E. & Peachey, J. 1999. Evidence for pre-Cretaceous rifting in the Rockall Trough: an analysis using quantitative plate tectonic modelling. *In*: Fleet, A.J. & Boldy, S.A.R. (eds) *Petroleum Geology of Northwest Europe: Proceedings of the 5th Conference*. Geological Society, London, 359–370, https://doi.org/10.1144/0050359

Cowie, L. & Kusznir, N.J. 2012*a*. Gravity inversion mapping of crustal thickness and lithosphere thinning for the eastern Mediterranean. *The Leading Edge*, **31**, 810–814.

Cowie, L. & Kusznir, N.J. 2012*b*. Mapping crustal thickness and oceanic lithosphere distribution in the Eastern Mediterranean using gravity inversion. *Petroleum Geoscience*, **18**, 373–380, https://doi.org/10.1144/petgeo2011-071

Cowie, L., Kusznir, N.J. & Manatschal, G. 2015. Determining the COB location along the Iberian margin and Galicia Bank from gravity anomaly inversion, residual depth anomaly and subsidence analysis. *Geophysical Journal International*, **203**, 1355–1372, https://doi.org/10.1093/gji/ggv367

Cowie, L., Angelo, R.M., Kusznir, N.J., Manatschal, G. & Horn, B. 2016. Structure of the ocean–continent transition, location of the continent–ocean boundary and magmatic type of the northern Angolan margin from integrated quantitative analysis of deep seismic reflection and gravity anomaly data. *In*: Sabato Ceraldi, T., Hodgkinson, R.A. & Backe, G. (eds) *Petroleum Geoscience of the West Africa Margin*. Geological Society, London, Special Publications, **438**, 159–176, https://doi.org/10.1144/SP438.6

Czarnota, K., Hoggard, M.J., White, N.J. & Winterbourne, J.R. 2013. Spatial and temporal patterns of Cenozoic dynamic topography around Australia, *Geochemistry Geophysics. Geosystems*, **14**, 634–658, https://doi.org/10.1029/2012GC004392

Davis, M.W., White, N.J., Priestley, K.F., Baptie, B.J. & Tilmann, F.J. 2012. Crustal structure of the British Isles and its epeirogenic consequences. *Geophysical Journal International*, **190**, 705–725, https://doi.org/10.1111/j.1365-246X.2012.05485.x

Dickin, A.P. 1992. Evidence for an Early Proterozoic crustal province in the North Atlantic region. *Journal of the Geological Society, London*, **149**, 483–486, https://doi.org/10.1144/gsjgs.149.4.0483

Divins, D.L. 2003. *Total Sediment Thickness of the World's Oceans & Marginal Seas*. NOAA National Geophysical Data Center, Boulder, CO, USA; updates http://www.ngdc.noaa.gov/mgg/sedthick/sedthick.html

Doré, A.G., Lundin, E.R., Jensen, L.N., Birkeland, Ø., Eliassen, P.E. & Fichler, C. 1999. Principal tectonic events in the evolution of the northwest European Atlantic margin. *In*: Fleet, A.J. & Boldy, S.A.R. (eds) *Petroleum Geology of Northwest Europe: Proceedings of the 5th Conference*. Geological Society, London, 41–61, https://doi.org/10.1144/0050041

England, R.W. 1995. Westline: a deep near-normal incidence reflection profile across the Rockall Trough. *In*: Croker, P.F. & Shannon, P.M. (eds) *The Petroleum Geology of Ireland's Offshore Basins*. Geological Society, London, Special Publications, **93**, 423–427, https://doi.org/10.1144/GSL.SP.1995.093.01.32

England, R.W. & Hobbs, R.W. 1997. The structure of the Rockall Trough imaged by deep seismic reflection profiling. *Journal of the Geological Society, London*, **154**, 497–502, https://doi.org/10.1144/gsjgs.154.3.0497

Fletcher, R.F., Kusznir, N.J., Roberts, A.M. & Hunsdale, R. 2013. The formation of a failed continental breakup basin: The Cenozoic development of the Faroe-Shetland Basin. *Basin Research*, **25**, 532–553, https://doi.org/10.1111/bre.12015

Greenhalgh, E.E. & Kusznir, N.J. 2007. Evidence for thin oceanic crust on the extinct Aegir Ridge, Norwegian Basin, NE Atlantic derived from satellite gravity inversion. *Geophysical Research Letters*, **34**, L06305, https://doi.org/10.1029/2007GL029440

Hauser, F., O'Reilly, B.M., Jacob, B., Shannon, P.M., Makris, J. & Vogt, U. 1995. The crustal structure of the Rockall Trough: Differential stretching without underplating. *Journal of Geophysical Research*, **100**, 4097–4116.

Hitchen, K., Johnson, H. & Gatliff, R.W. (eds). 2013. *Geology of the Rockall Basin and Adjacent Areas*. British Geological Survey Research Report RR/12/03. British Geological Survey, Nottingham, UK.

Jones, S.M., White, N., Clarke, B.J., Rowley, E. & Gallagher, K. 2002. Present and past influence of the Iceland Plume on sedimentation. *In*: Doré, A.G., Cartwright, J.A., Stoker, M.S., Turner, J.P. & White, N. (eds) *Exhumation of the North Atlantic Margin: Timing, Mechanisms and Implications for Petroleum Exploration*. Geological Society, London, Special Publications, **196**, 13–25, https://doi.org/10.1144/GSL.SP.2002.196.01.02

Joppen, M. & White, R.S. 1990. The structure and subsidence of Rockall Trough from two-ship seismic experiments. *Journal of Geophysical Research*, **95**, 19 821–19 837.

Kelly, A., England, R.W. & Maguire, P.K.H. 2007. A crustal seismic velocity model for the UK Ireland and surrounding areas. *Geophysical Journal International*, **171**, 1172–1184, https://doi.org/10.1111/j.1365-246X.2007.03569.x

Keser Neish, J.K. 1993. Seismic structure of the Hatton–Rockall area: an integrated seismic/modelling study from composite datasets. *In*: Parker, J.R. (ed.) *Petroleum Geology of Northwest Europe: Proceedings of the 4th Conference*. Geological Society, London, 1047–1056, https://doi.org/10.1144/0041047

Kimbell, G. S., Gatliff, R. W., Ritchie, J. D., Walker, A. S. D. & Williamson, J. P. 2004. Regional three-dimensional gravity modelling of the NE Atlantic margin. *Basin Research*, **16**, 259–278, https://doi.org/10.1111/j.1365-2117.2004.00232.x

Kimbell, G.S., Ritchie, J.D., Johnson, H. & Gatliff, R.W. 2005. Controls on the structure and evolution of the NE Atlantic margin revealed by regional potential field imaging and 3D modelling. *In*: Doré, A.G. & Vining, B.A. (eds) *Petroleum Geology: North-West Europe and Global Perspectives – Proceedings of the 6th Petroleum Geology Conference*. Geological Society, London, 933–945, https://doi.org/10.1144/0060993

Kimbell, G.S., Stewart, M.A. *et al.* 2017. Controls on the location of compressional deformation on the NW European margin. *In*: Péron-Pinvidic, G., Hopper, J.R., Stoker, M.S., Gaina, C., Doornenbal, J.C., Funck, T. & Árting, U.E. (eds) *The NE Atlantic Region: A Reappraisal of Crustal Structure, Tectonostratigraphy and Magmatic Evolution*. Geological Society, London, Special Publications, **447**, 249–278, https://doi.org/10.1144/SP447.3

Klingelhöfer, F., Edwards, R.A., Hobbs, R.W. & England, R.W. 2005. Crustal structure of the NE Rockall Trough from wide-angle seismic data modelling. *Journal of Geophysical Research*, **110**, B11105, https://doi.org/10.1029/2005JB003763

Kusznir, N.J., Roberts, A.M. & Morley, C. 1995. Forward and reverse modelling of rift basin formation. *In*: Lambiase, J. (ed.) *Hydrocarbon Habitat in Rift Basins*. Geological Society, London, Special Publications, **80**, 33–56, https://doi.org/10.1144/GSL.SP.1995.080.01.02

Kusznir, N.J., Hunsdale, R. & Roberts, A.M. & iSIMM Team. 2005. Timing and magnitude of depth-dependent lithosphere stretching on the southern Lofoten and northern Vøring continental margins offshore mid-Norway: implications for subsidence and hydrocarbon maturation at volcanic rifted margins. *In*: Doré, A.G. & Vining, B.A. (eds) *Petroleum Geology: North-West Europe and Global Perspectives – Proceedings of the 6th Petroleum Geology Conference*. Geological Society, London, 767–783, https://doi.org/10.1144/0060767

Kusznir, N.J., Roberts, A.M. & Alvey, A.D. 2018. Crustal structure of the conjugate Equatorial Atlantic Margins, derived by gravity anomaly inversion. *In*: McClay, K.R. (ed.) *Passive Margins: Tectonics, Sedimentation and Magmatism*. Geological Society, London, Special Publications, **476**, first published online March 19, 2018, https://doi.org/10.1144/SP476.5

Lundin, E.R. & Doré, A.G. 2011. Hyperextension, serpentinization, and weakening: A new paradigm for rifted margin compressional deformation. *Geology*, **39**, 347–350, https://doi.org/10.1130/G31499.1.

McKenzie, D.P. 1978. Some remarks on the development of sedimentary basins. *Earth and Planetary Science Letters*, **40**, 25–32.

McKenzie, D.P. & Bickle, M. J. 1988. The volume and composition of melt generated by extension of the lithosphere. *Journal of Petrology*, **29**, 625–679.

Morewood, N.C., Mackenzie, G.D., Shannon, P.M., O'Reilly, B.M., Readman, P.W. & Makris, J. 2005. The crustal structure and regional development of the Irish Atlantic margin region. *In*: Doré, A.G. & Vining, B.A. (eds) *Petroleum Geology: North-West Europe and Global Perspectives – Proceedings of the 6th Petroleum Geology Conference*. Geological Society, London, 1023–1033, https://doi.org/10.1144/0061023

Musgrove, F.W. & Mitchener, B. 1996. Analysis of the pre-Tertiary rifting history of the Rockall Trough. *Petroleum Geoscience*, **2**, 353–360, https://doi.org/10.1144/petgeo.2.4.353

Nadin, P.A. & Kusznir, N.J. 1995. Palaeocene uplift and Eocene subsidence in the northern North Sea Basin from 2D forward and reverse stratigraphic modelling. *Journal of the Geological Society, London*, **152**, 833–848, https://doi.org/10.1144/gsjgs.152.5.0833

Nadin, P.A., Kusznir, N.J &Toth, J. 1995. Transient regional uplift in the Early Tertiary of the northern North Sea and the development of the Iceland Plume. *Journal of the Geological Society, London*, **152**, 953–958, https://doi.org/10.1144/GSL.JGS.1995.152.01.12

Nadin, P.A., Kusznir, N.J. & Cheadle, M.J. 1997. Early Tertiary plume uplift in the North Sea and Faeroe–Shetland Basin. *Earth and Planetary Science Letters*, **148**, 109–127.

Nadin, P.A., Houchen, M.A. & Kusznir, N.J. 1999. Evidence for pre-Cretaceous rifting in the Rockall Trough: an analysis using quantitative 2D structural/stratigraphic modelling. *In*: Fleet, A.J. & Boldy, S.A.R. (eds) *Petroleum Geology of Northwest Europe: Proceedings of the 5th Conference*. Geological Society, London, 371–378, https://doi.org/10.1144/0050371

Ritchie, J.D. & Hitchen, K. 1996. Early Paleogene offshore igneous activity to the northwest of the UK and its relationship to the North Atlantic Igneous Province. *In*: Knox, R.W.O'B., Corfield, R.M. & Dunay, R.E. (eds) *Correlation of the Early Paleogene in Northwest Europe*. Geological Society, London, Special Publications, **101**, 63–78, https://doi.org/10.1144/GSL.SP.1996.101.01.04

Ritchie, J.D., Gatliff, R.W. & Richards, P.C. 1999. Early Tertiary magmatism in the offshore NW UK margin and surrounds. *In*: Fleet, A.J. & Boldy, S.A.R. (eds) *Petroleum Geology of Northwest Europe: Proceedings of the 5th Conference*. Geological Society, London, 573–584, https://doi.org/10.1144/0050573

Ritchie, J.D., Johnson, H., Kimbell, G.S. & Quinn, M. 2013. Structure. *In*: Hitchen, K., Johnson, H. & Gatliff, R.W. (eds) *Geology of the Rockall Basin and Adjacent Areas*. British Geological Survey Research Report RR/12/03. British Geological Survey, Nottingham, UK, 10–46.

Roberts, A.M., Lundin, E.R. & Kusznir, N.J. 1997. Subsidence of the Vøring Basin and the influence of the Atlantic continental margin. *Journal of the Geological Society, London*, **154**, 551–557, https://doi.org/10.1144/gsjgs.154.3.0551

Roberts, A.M., Kusznir, N.J., Yielding, G. & Styles, P. 1998. 2D flexural backstripping of extensional basins; the need for a sideways glance. *Petroleum Geoscience*, **4**, 327–338, https://doi.org/10.1144/petgeo.4.4.327

Roberts, A.M., Corfield, R.I., Kusznir, N.J., Matthews, S.J., Kåre-Hansen, E. & Hooper, R.J. 2009. Mapping palaeostructure and palaeobathymetry along the Norwegian Atlantic continental margin: Møre and Vøring Basins. *Petroleum Geoscience*, **15**, 27–43, https://doi.org/10.1144/1354-079309-804

Roberts, A.M., Kusznir, N.J., Corfield, R.I., Thompson, M. & Woodfine, R. 2013. Integrated tectonic basin modelling as an aid to understanding deep-water rifted continental margin structure and location. *Petroleum Geoscience*, **19**, 65–88, https://doi.org/10.1144/petgeo2011-046

Roberts, D.G., Ginzberg, A., Nunn, K. & McQuillin, R. 1988. The structure of the Rockall Trough from seismic refraction and wide-angle reflection measurements. *Nature*, **332**, 632–635.

Sandwell, D. T. & Smith, W.H.F. 2009. Global marine gravity from retracked Geosat and ERS-1 altimetry: Ridge Segmentation versus spreading rate. *Journal of Geophysical Research*, **114**, B01411, https://doi.org/10.1029/2008JB006008; updates http://topex.ucsd.edu/WWW_html/mar_grav.html.

Schofield, N., Jolley, J. *et al.* 2017. Challenges of future exploration within the UK Rockall Basin. *In*: Bowman, M. & Levell, B. (eds) *Petroleum Geology of NW Europe: 50 Years of Learning – Proceedings of the 8th Petroleum Geology Conference*. Geological Society, London, 211–229, https://doi.org/10.1144/PGC8.37

Sclater, J.G. & Christie, P A.F. 1980. Continental Stretching: an explanation of the post mid-Cretaceous subsidence of the Central North Sea Basin. *Journal of Geophysical Research*, **85**, 3711–3739.

Sclater, J.G., Jaupart, C. & Galson, D. 1980. The heat flow through oceanic and continental crust and the heat loss of the Earth. *Reviews of Geophysics*, **18**, 269–311, https://doi.org/10.1029/RG018i001p00269

Shannon, P.M., Jacob, A.W.B., O'Reilly, B.M., Hauser, F., Readman, P.W. & Makris, J. 1999. Structural setting, geological development and basin modelling in the Rockall Trough. *In*: Fleet, A.J. & Boldy, S.A.R. (eds) *Petroleum Geology of Northwest Europe: Proceedings of the 5th Conference*. Geological Society, London, 421–431, https://doi.org/10.1144/0050421

Sibuet, J.-C., Srivastava, S.P., Enachescu, M. & Karner, G.D. 2007. Early Cretaceous motion of Flemish Cap with respect to North America: implications on the formation of Orphan Basin and SE Flemish Cap–Galicia Bank conjugate margins. *In*: Karner, G.D., Manatschal, G. & Pinheiro, L.M. (eds) *Imaging, Mapping and Modelling Continental Lithosphere Extension and Breakup*. Geological Society, London, Special Publications, **282**, 63–76, https://doi.org/10.1144/SP282.4

Smith, K. 2013. Cretaceous. *In*: Hitchen, K., Johnson, H. & Gatliff, R.W. (eds) *Geology of the Rockall Basin and Adjacent Areas*. British Geological Survey Research Report RR/12/03. British Geological Survey, Nottingham, UK, 71–80.

Smith, R.A. 1961. A uniqueness theorem concerning gravity fields. *Proceedings of the Cambridge Philosophical Society*, **57**, 865–870.

Smith, W. H. F. & Sandwell, D.T. 1997. Global seafloor topography from satellite altimetry and ship depth soundings. *Science*, **277**, 1957–1196; updates http://topex.ucsd.edu/marine_topo/.

Smythe, D.K. 1989. Rockall Trough – Cretaceous or Late Palaeozoic? *Scottish Journal of Geology*, **25**, 5–43, https://doi.org/10.1144/sjg25010005

Steinberg, J., Roberts, A.M., Kusznir, N.J., Schafer, K. & Karcz, Z. 2018. Crustal structure and post-rift evolution of the Levant Basin. *Marine and Petroleum Geology*, **95**, https://doi.org/10.1016/j.marpetgeo.2018.05.006

Stoker, M.S., Stewart, M.A. *et al.* 2017. An overview of the Upper Palaeozoic–Mesozoic stratigraphy of the NE Atlantic region. *In*: Péron-Pinvidic, G., Hopper, J.R., Stoker, M.S., Gaina, C., Doornenbal, J.C., Funck, T. & Árting, U.E. (eds) *The NE Atlantic Region: A Reappraisal of Crustal Structure, Tectonostratigraphy and Magmatic Evolution*. Geological Society, London, Special Publications, **447**, 11–68, https://doi.org/10.1144/SP447.2

Stuevold, L.M., Skogseid, J. & Eldholm, O. 1992. Post-Cretaceous uplift events on the Vøring continental margin. *Geology*, **20**, 919–922.

Tuitt, A., Underhill, J.R., Ritchie, J.D., Johnson, H. & Hitchen, K. 2010. Timing, controls and consequences of compression in the Rockall–Faroe area of the NE Atlantic margin. *In*: Vining, B. & Pickering, S. (eds) *Petroleum Geology: From Mature Basins to New Frontiers – Proceedings of the 7th Petroleum Geology Conference*. Geological Society, London, 963–977, https://doi.org/10.1144/0070963

Vitorello, I. & Pollack, H.N. 1980. On the variation of continental heat flow with age and the thermal evolution of continents. *Journal of Geophysical Research*, **85**, 983–995, https://doi.org/10.1029/JB085iB02p00983.

Warner, M.R. 1987. Seismic reflections from the Moho – the effect of isostasy. *Geophysical Journal of the Royal Astronomical Society*, **88**, 425–435.

White, R.S. & McKenzie, D.P. 1989. Magmatism at rift zones: the generation of volcanic continental margins and flood basalts. *Journal of Geophysical Research*, **94**, 7685–7729.

White, R.S., Eccles, J.D. & Roberts, A.W. 2010. Constraints on volcanism, igneous intrusion and stretching on the Rockall–Faroe continental margin. *In*: Vining, B. & Pickering, S. (eds) *Petroleum Geology: From Mature Basins to New Frontiers – Proceedings of the 7th Petroleum Geology Conference*. Geological Society, London, 831–842, https://doi.org/10.1144/0070831

Winterbourne, J.R., Crosby, A.G. & White, N.J. 2009. Depth, age and dynamic topography of oceanic lithosphere beneath heavily sedimented Atlantic margins. *Earth and Planetary Science Letters*, **287**, 137–151, https://doi.org/10.1016/j.epsl.2009.08.019

Winterbourne, J.R., White, N.J. & Crosby, A.G. 2014. Accurate measurements of residual topography from the oceanic realm. *Tectonics*, **33**, 982–1015, https://doi.org/10.1002/2013TC003372